2005

SYMLET AND GABOR WAVELET PREDICTION OF PRINT DEFECTS

Elios Klemo
University of Kentucky, eklemous@yahoo.com

ABSTRACT OF THESIS

SYMLET AND GABOR WAVELET PREDICTION OF PRINT DEFECTS

Recent studies have been done to create models that predict the response of the human visual system (HVS) based on how the HVS processes an image. The most widely known of these models is the Gabor model, since the Gabor patterns closely resemble the receptive filters in the human eye. The work of this thesis examines the use of Symlets to represent the HVS, since Symlets provide the benefit of orthogonality. One major problem with Symlets is that the energy is not stable in respective Symlet channels when the image patterns are translated spatially. This thesis addresses this problem by up sampling Symlets instead of down sampling, and thus creating shift invariant Symlets. This thesis then compares the representation of Gabor versus Symlet approach in predicting the response of the HVS to detecting print defect patterns such as banding and graining. In summary we noticed that Symlet prediction outperforms the Gabor prediction thus Symlets would be a good choice for HVS response prediction. We also concluded that for banding defect periodicity and size are important factors that affect the response of the HVS to the patterns. For graining defects we noticed that size does not greatly affect the response of the HVS to the defect patterns. We introduced our results using two set of performance metrics, the mean and median.

KEYWORDS: Symlet, Gabor, Human Vision, Psychometric Test, Print Defects

Elios Klemo

December 12, 2005.

SYMLET AND GABOR WAVELET PREDICTION OF PRINT DEFECTS

By

Elios Klemo

Dr. Kevin D. Donohue
(Director of Thesis)

Dr. YuMing Zhang
(Director of Graduate Studies)

December 12, 2005

RULES FOR THE USE OF THESES

Unpublished theses submitted for the Master's degree and deposited in the University of Kentucky Library are as a rule open for inspection, but are to be used only with due regard to the rights of the authors. Bibliographical references may be noted, but quotations or summaries of parts may be published only with the permission of the author, and with the usual scholarly acknowledgments.

Extensive copping or publication of the thesis in whole or in part also requires the consent of the Dean of the Graduate school of the University of Kentucky.

A library that borrows this thesis for use by its patrons is expected to secure the signature of each user.

Name Date

THESIS

Elios Klemo

The Graduate School

University of Kentucky

2005

SYMLET AND GABOR WAVELET PREDICTION OF PRINT DEFECTS

THESIS

A thesis submitted in partial fulfillment of the
requirements for the degree of Master of Science in the
College of Engineering
at the University of Kentucky

By

Elios Klemo

Lexington, Kentucky

Director: Dr. Kevin D. Donohue, Associate Professor of
Electrical Engineering, Lexington, Kentucky

2005

DEDICATION

To Lefter, Liliana, Migena

ACKNOWLEDGEMENTS

I would like to thank Dr. Kevin Donohue for his support and guidance with this thesis. His input was a corner stone in my understanding and completion of this thesis. I was very lucky to be given the opportunity to work for Dr. Donohue. Your insight helped me better understand this subject and also it ignited my desire to work in the field of image processing.

I would also like to thank the support of Lexmark International and their gift for this research.

I would like to thank my lab mates Il-Won Shin, Nathir, and Vijay for their patience and great team spirit. I cherish the experience of working with all of you.

TABLE OF CONTENTS

LIST OF TABLES

LIST OF FIGURES

LIST OF FILES

EKThesis.pdf……552KB

CHAPTER 1

Introduction and Literature Review

An area of image processing involves understanding the response of the Human Visual System and modeling the response with computational algorithms that operated on the image function. An understanding of the human visual system is beneficial for creating images for optimal presentation of information and human appreciation. Image quality is an important factor that greatly influences the field of image signal processing.
In recent years a great emphasis is given to developing image quality metrics. If these metrics can be correlated to the human judgment response, they can serve as a common standard for making image quality assessments and comparison. The literature review included in this thesis gives an overview of previous work related to this thesis. This thesis describes two different methods used to predict the human's visual system response to defect patterns such as graining and banding. The 2 methods are based on Symlet and Gabor decompositions of images to model the independent visual pathways or channels that carry stimuli to the visual cortex.

1.1 Image Quality

This is the era of digital information technology. Demand has increased rapidly for complex interactive media communication including voice and video images. The information content has increased tremendously and visual images are the most demanding component relative to bandwidth needs. This increase in visual imagery has lead to creation of lossless and lossy compression in order to reduce the burden of the bandwidth demand. An image presented to an observer may have undergone considerable changes in order to reduce bandwidth, storage space, and processing time. For example, when a picture is taken using a digital camera, several errors are introduced such as optics error, focus error, noise etc. The picture image is also compressed to save memory space before it is shown to the observer. All these transformations can reduce image quality. Image quality can also vary depending on the application [1]. For example, images for conference calls require lower quality than medical MRI scans. The final goal in image

compression is reduction in bandwidth while preserving image quality. In order to achieve this, a better understanding of Human Visual System and image perception is required.

A step in better understanding of Human Visual System includes understanding the human perception of print defect patterns such as graining and banding. Understanding how the visual system perceives defects helps in better understanding of image quality. An improvement of image quality first starts with a solid understanding of the visual perception.

1.2 Human Visual System (HVS)

The area of Vision Research focuses on understanding the HVS and how it responds to various visual stimuli. If an image can be decomposed into a set of basis functions modeling the independent visual channels of the Human Visual System response, one can potentially predict or mimic the response to that image from the individual channel responses (at least for pattern detection). Understanding the HVS system leads to improvement in image quality.

Electrophysiology and Psychophysics are areas concerned with understanding the HVS. Electrophysiology is concerned with neurological structure and organization, while psychophysics is concerned with how the HVS system perceives information [2]. Various studies are done to design models that successfully predict visual perception [3-5]. These studies have combined various psychophysical and electro physical data to create these models. The models are created by finding a detection threshold, which is the limit above which perceptual image quality decreases. Visual detection is modeled as a set of spatial filters based on these threshold measurements.

1.3 HVS models

The traditional way of measuring image quality is the signal-to-noise ratio (SNR)[1,2].There are many problems with this procedure, a critical one being that it does

not provide a scale for human perception of image quality. The emphasis or current research creates a measure of image quality based on properties of HVS [1,2,4,6].
The properties incorporated into HVS models are; sensitivity to luminance variations, spatial frequency sensitivity, and effects of masking.
Human eye sensitivity to luminance differences is relative to the background luminance. Spatial frequency sensitivity is characterized by the Contrast Sensitivity Function (CSF). The figure below illustrates the CSF.

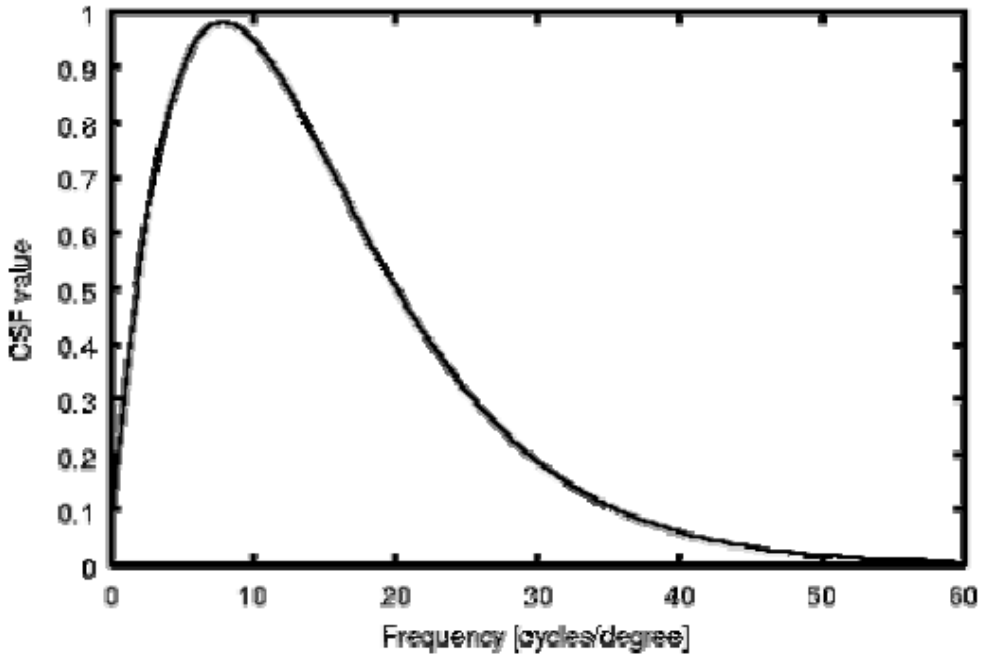

Figure 1.1 Contrast Sensitivity curve as a function of frequency adapted from [7]

Contrast sensitivity score is a reciprocal measure of visual threshold (1/threshold). All contrast sensitivity scores are plotted as a function of spatial frequencies resulting in Contrast Sensitivity Function (CSF). As it can be observed from the figure the CSF is much more sensitive at mid spatial frequencies and much less sensitive at low and high spatial frequencies. The spatial frequency units of CSF are cycles/degrees [7, 8].

1.3.1 The need for a library of HVS models

Years of research work in HVS has created a wide range of models for the visual receptors [1,2,4,5,6]. This wide range of different models also has created a wide range of

data sets making it difficult to utilize these models. To address these issues an organization referred to as ModelFest was formed to create standards for experimental procedures and testing models associated with HVS research [1]. The ModelFest created a reference model database of test images obtained from different laboratories. The threshold results of these image sets will also be recorded in the database. This set of data will be used to design and test HVS models. Currently only static gray scale two dimensional images are considered. In the future the database will include more complex patterns as well as thresholds for color and gray scale images. "The goal is to provide a readily available stimulus database designed to test many different aspects of the HVS models". [1] The benefit of this database is that for every available stimulus there will be one available corresponding threshold results. This will be useful for building new models and comparing existing models performance.

The most common stimuli used in ModelFest database to predict the perception of HVS are Gabor patterns, Gabor plaids, Gaussian blobs, multipoles and white noise. Gabor Patterns are the most commonly used to represent independent visual channel responses. This is due to its localization properties in both spatial and frequency domain. This allows Gabor functions to perform multi-resolution decomposition.
Various studies have shown that the Gabor patterns closely match the response of receptive fields of neurons in visual cortex. [1,9,10,11]. Also, various experiments where done that resulted in Gabor models achieving the best results for creating HVS models. The ModelFest database lists all the models tested [1]. The first category in the database contains five categories of Gabor patches varying in bandwidth, frequency, aspect ratio and orientations.

The next category contains a combination of Gabor patches for different frequencies and phases. Gaussian blobs stimuli are used in order to examine Ricco's area (the area of complete summation), low frequencies and orientation. Multipoles will examine edges lines and dipoles. This research focuses on Gabor patterns only. To be more specific the patterns used in this research are Gabor patches with fixed size in cycles, and fixed size in degrees. The construction of Gabor filters is explained in details in Chapter 2 of this

thesis. The Gabor filters where constructed using the guidelines set by Modelfest. One of the goals of these patterns is to help us map the visual perception of printer defects.

1.4 Print Defect Characterization

Printer defects have an impact on printer quality. In order to improve printer quality it is necessary to provide a characterization of common printer defects. The most common printer defects include banding, striking, graininess and mottle. Efficient characterization of print defects with a potential for correlation with perceptual response means characterizing defects in a way that mimics the visual system response.

Many models are created to characterize print defects. Such models are shown by Brigs and Kane [12,13]. One problem with these models is they do not take in account human perception while evaluating printer defects. Human perception of printer defects is an integral part of defect detection process. With help of groups like ModelFest it is possible to correlate analysis of defect patterns with human perception, resulting in better and more effective characterization of these defects.

Since HVS properties are defined in frequency domain, the most commonly used models are also in frequency domain. This models use Fourier based method to characterize HVS properties. This research is concerned with characterization of two print defect models, banding and graining defects. These defects are the most common types found in printed samples. They can greatly influence the quality of printed samples. This thesis characterizes the banding and graining defects based on Gabor and Symlet HVS models. The section that follows describes in more details the two models used in this thesis.

1.4.1 HVS models Gabor vs. Symlets

Gabor models have lately been a preferable choice in testing visual perception due to their localization properties in frequency and spatial domains. Research has indicated that receptive fields of cortical simple cells can be described by a Gabor function. Marcelja and Daugman where among the first to suggest this relation [9,10,11]. Many studies in psychophysics and visual neuroscience make use of this general model. An impressive

study performed by Palmer and Jones showed that a 2D Gabor function match very closely receptive fields (RF) profile [14]. There have also been several dissenting views of this hypothesis. For example Stork and Wilson concluded that the Gabor function model is not well supported [15]. Despite the contrary views most researchers in the field of image processing accept the Gabors as a close representation of RF.

Recently effort is being made to characterize printing defects by Symlet analysis. From studies it is determined that perception channels of HVS are octave base spread in frequency domain. The dyadic Symlet-based decomposition is also octave based. The purpose of this research is to determine whether Symlets can provide a good approximation of the HVS system similar like Gabor patterns. One of the major benefits of being able to use Symlets to approximate the HVS over Gabor is their orthogonality property which provides computational efficiency for signals with localized space-frequency properties such as banding defects. In addition, orthogonality implies that adjacent Symlet channels do not share common image energy as the Gabor channels do, which leads to double counting the image energy. Also another advantage is that Symlets have several choices of transform kernels. Previous work in Symlet characterization of print defect patterns was done by Venkantesh and Donohue[17]. In their work Venkantesh and Donohue observed how printer defects such as graining and banding appear in wavelet domain. They also indicated the Symlets transforms the common defect patterns into fewer significant coefficients than other sine-based transforms. Thus prediction of detecting patterns based on the human responses to the basis function, does not have to be as highly dependent on the pooling algorithms that attempt to mimic higher-level visual function that combine coefficient from different channels.

In contrast from Venkantesh and Donohue research, this thesis follows a different approach for Symlet characterization. This approach includes upsampling of Symlet coefficients instead of the traditional downsampling approach. Also, due to up-sampling Symlet shiftability in time domain is not any more a concern as in the case of Venkantesh thesis [16]. Venkatesh in his research noticed that if Symlet basis functions where shifted

in time that resulted in loss of energy within subands. This is better explained in chapter 2 of this thesis. Up-sampling guarantees preservation of energy within subands.
Venkantesh in his thesis work used sinusoidal and Symlet models to characterize print defect patterns. He was able to predict the HVS response to print defect patterns around the visual threshold point of these defects. In this thesis we were able to predict the response not just for the HVS threshold, but for the all contrast axis.
Both the Symlet and Gabor models used in this thesis are discussed in details in chapter 2 of this thesis.

1.5 Hypothesis

The objective of this thesis is predicting the perception of banding and graining defect by Symlet and Gabor approach, and comparing the performance of the two with subjective testing results. Subjective test was designed to test feasibility of this prediction and to determine which approach Symlet or Gabor yields better results. Also metrics such as mean and median were designed to help assess the prediction process.

1.6 Organization of the thesis

This chapter set the road map for this thesis. Chapter 2 discusses the design of the subject test and stimuli design. Chapter 3 discusses prediction procedure followed and analysis of the data obtained from subject test. Chapter 4 shows the obtained final results from the experiments and discussion of these results.
Chapter 5 presents future work to be done in this area of research.

CHAPTER 2

Experimental Design

A set of tools is needed to obtain HVS models for defect patterns such as graining and banding described in chapter 1. These tools include visual tests as well as the creation of a library of basis functions and defect patterns to be tested. This chapter discusses the set toolkit used to obtain characterization of print defect patterns and the basis functions described in chapter 1 that will lay the frame work for building the HVS models.
Two kinds of basis functions were used in the prediction process, Symlet and Gabor functions. The prediction process involves characterization of HVS response to defect patterns. The results from the prediction process are compared with results from subject testing. The simulated defect patterns include banding and graining patterns. The design flow chart below describes the flow of the research. This chapter will discuss the first three boxes of the flow chart shown in figure 2.1.

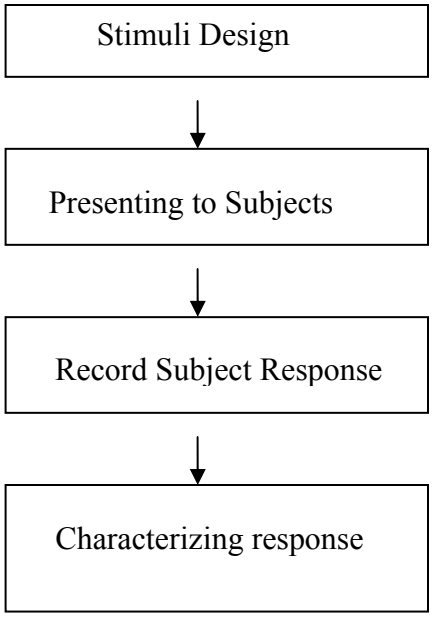

Figure 2.1 Flow chart of Research Project

2.1 Stimuli Design

Four kinds of stimuli were presented to the subjects, Gabor stimuli, Symlet stimuli and banding and graining defect stimuli. This section describes how each of the stimuli was constructed and how the HVS threshold predictions was obtained from these stimuli.

2.1.1 Gabor Stimuli

The Gabor Stimuli was constructed by multiplying a Gaussian function with a sinusoid function. The Gabor Stimuli provide a map of the human visual system that is most commonly used in vision research. This section describes the procedure used to obtain the Gabor basis functions.

A 2-D cosine function in the XY-plane was defined as:

$$b(X, Y, f) = \cos(2\pi(f\cos(\theta)X + f\sin(\theta)Y)) \tag{2.1.1}$$

where f is the sinusoid frequency, θ is the angle of rotation in three directions vertical, horizontal and diagonal. X and Y represent the spatial axis in pixels. As described later in this chapter a LCD monitor was used to conduct the test, thus pixels are the appropriate metrics that describe Cartesian coordinates.

Let the Gaussian envelope be defined as:

$$g(X,Y;\theta,S_x,S_y) = \exp\left(-((\cos(\theta)\frac{X}{S_x})^2 + (\cos(\theta)\frac{X}{S_y})^2 + (\sin(\theta)\frac{Y}{S_x})^2 + (\sin(\theta)\frac{Y}{S_y})^2)\right) \tag{2.1.2}$$

where S_x and S_y represent the variance along x and y direction.

The Resulting Gabor function would be:

$$G(X,Y;\theta,S_x,S_y) = g(X,Y,\theta,S_x,S_y) * b(X,Y,f) \tag{2.1.3}$$

The resulting Gabor function in three orientations is shown in the figure 2.2 below.

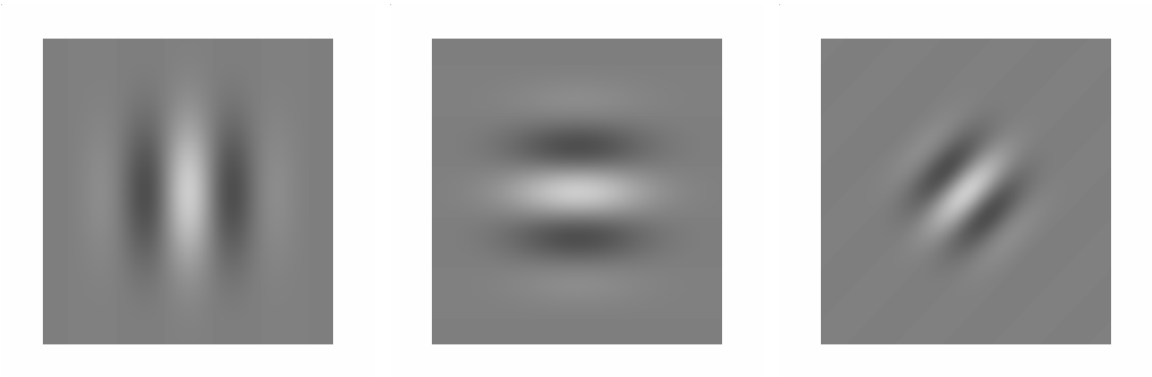

Figure 2.2 Gabor Stimuli in three orientations; vertical, horizontal and diagonal

The Contrast Sensitivity Function was introduced in chapter 1. The range of HVS detectable frequencies is from 0-60 cycles per degree. As it is described in chapter 1 the CSF is much more sensitive at mid spatial frequencies and much less sensitive at low and high spatial frequencies. Thus the selected frequency range of the basis functions should be such so that it would cover the mid spatial frequencies. This range corresponds to frequencies of [1.40, 2.81, 5.62, 11.25, 22.5] cycles/degree (CPD). These frequencies were selected following guidelines from ModelFest Group [1]. This range of frequencies allows for better coverage of the CSF spectrum and thus a better understanding of the response of HVS to defect patterns for various visible frequency ranges. The frequencies are increased in octaves to provide better coverage of the whole HVS spectrum.

2.1.2 Symlet Stimuli

It is documented that Gabor patterns map very closely the human visual channels. One problem with Gabor patterns is that they are not orthogonal. Certain Symlets provide the benefit of orthogonality, which does not redundantly map energy from the original image into multiple bands. On the other hand, the Symlets ability to represents signals with a set of basis functions that are related by translation is an appealing characteristic.

There is one problem you have to overcome when using Symlets. Since the basis functions are related by translation and dilation we would expect the Symlet transform coefficients to behave in a similar manner as the basis function when translated. However this is not the case. In his work Simoncelli determined that if the input signal is translated

one sample to the left or right the distribution of the coefficients of the transform over the bands would change dramatically. He determined that the representation was dependent of alignment of input signal with the subsampling subands. This creates a problem in predicting the response of HVS, since we would like to see consistency in transform coefficients. Thus we would like to have translation-invariant coefficients. That is our decomposition coefficients should be invariant of any shift in the basis function. We can't expect consistency in a system that is based on convolution and subsampling. However, we can create a version of translation invariance by preserving the information within suband as the input signal is translated. Thus the energy within the suband will be preserved. In order to achieve this, the coefficients must be upsampled instead of downsamped. According to Simoncelli the shiftability constraint is equivalent to the constraint that the energy of the transform coefficients within suband is preserved when the input signal is shifted. In order for this statement to hold true the following proposition must hold.

- Given a set of transform coefficients y[n] the transform is shiftable if the power of the coefficients $\sum_{n=0}^{N-1}[y[n]]^2$ is invariant for translations of the input signal *f(x)*.

Thus the power should be equal to:

$$\sum_{n=0}^{N-1}\left|y[n]\right|^2 = \sum_{k=0}^{N-1}\sum_{l}\left|H(k+IN)\right|^2\left|F(k+IN)\right|^2 \qquad (2.1.4)$$

where *y[n]* represents the transform coefficients. *N* represents the number of transform coefficients, *k* represents the set of frequencies. *I* represent the set of integers. In order to preserve the energy within subands and form shiftable transforms the Symlet coefficients where upsampled for each level of decomposition. The Symlet frequencies were picked to match the Gabor frequencies. That is levels 2-6 were tested with frequencies [1.40, 2.81, 5.62, 11.25, 22.5] CPD. The stimuli for the Symlet basis function consisted of a 2-dimensional 8th order Symlet generated by placing a unit value in a position corresponding to a 6 level DWT transform 256x256 zero vector and reconstructing the vector using inversed DWT of the signal. The resulting pattern is the impulse response of the Symlet filters used to decompose the original image to coefficients at this that level. Level one of decomposition filters the image energy in to a band ranging from fs/4 to the Nyquist frequency (fs/2). For each subsequent level the frequency range is halved

due to the octave based frequency division nature of the Symlets. The Nyquist frequency corresponds to 60 cycles per degree. This Nyquist rate was obtained by following Model Fest guidelines of 0.5min pixel width. This frequency is determined taking into account seating distance as well as monitor resolution. This is covered in more details in Section 2.1.3. The Symlet basis functions were formed in three spatial orientations, horizontal, vertical and diagonal.

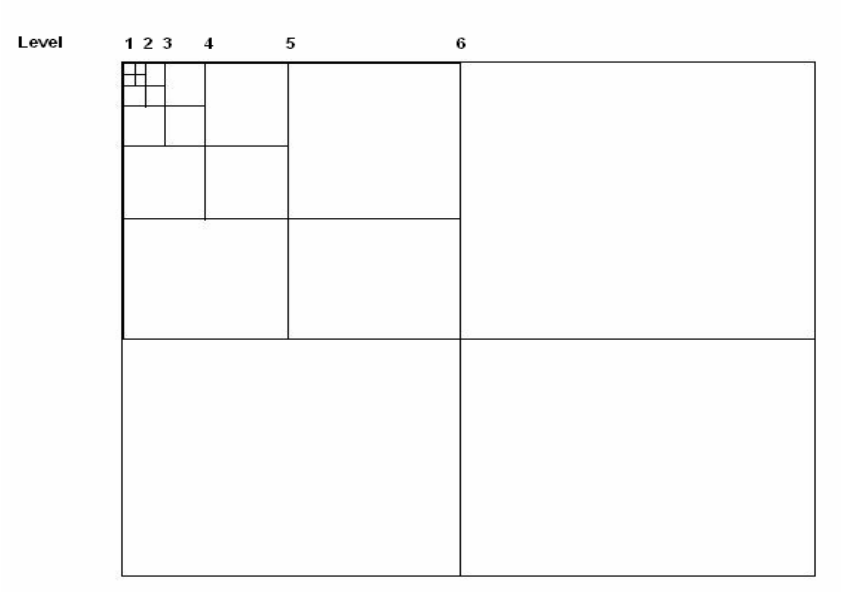

Figure 2.3 6-level Symlet decomposition

The Symlet stimuli in three orientations are shown in figure 2.4 for a particular level. The same shape is preserved from one band to the next; however the size of the patterns increase (or resolution decrease) supported by more pixels in the image.

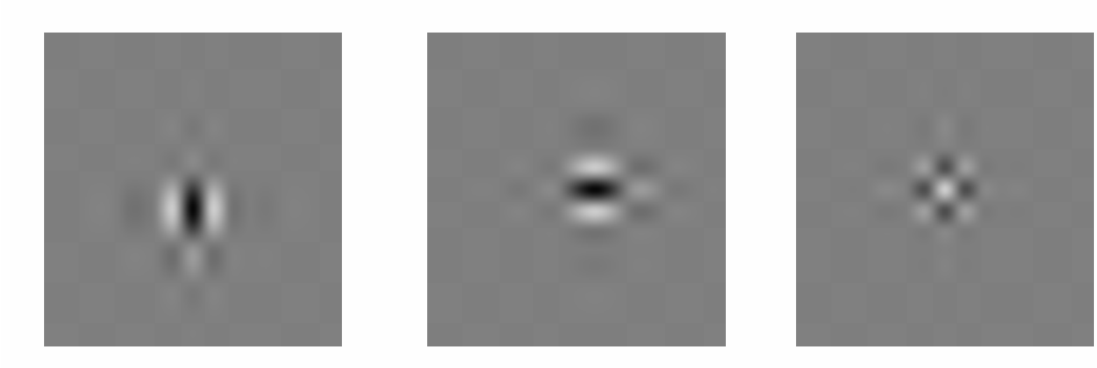

Figure 2.4 Symlet Stimuli (vertical, horizontal and diagonal orientations)

2.1.3 Defect Patterns

The defect patterns presented in the Subject Test include banding and graining patterns.

Banding Pattern:

Banding defects are periodic one dimensional fluctuation in darkness. The banding patterns were generated using documented banding defects from scanned images. The printed samples where taken from a Lexmark Z43 printer. Using interpolation the scanned image was stretched or compressed to create defects at various frequencies and contrast levels. For our research purpose we selected two frequencies for banding patterns at 4 and 8 CPD. In order to account for edge effects for each frequency, two Gaussian envelope sizes were selected. Figure 2.5 shows a banding defect for a frequency of 4 CPD and 8 CPD for two different envelope sizes. The frequencies of the banding patterns where chosen so they can be included within the Symlet patterns frequency spectra.

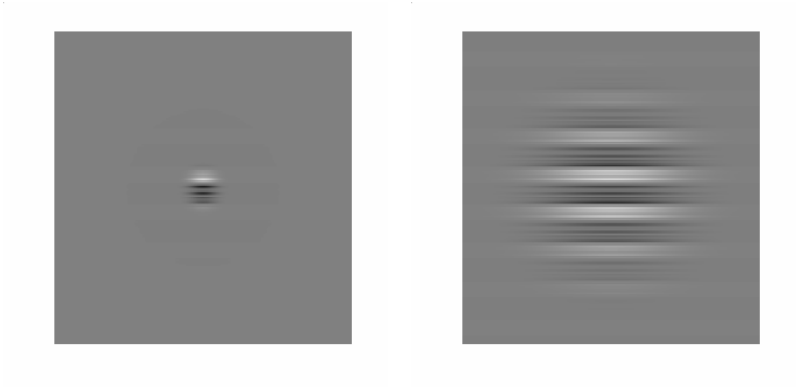

Figure 2.5 Banding patterns at 4 and 8 CPD and two envelope sizes, large and small

Grain Patterns:

Graining is defined to be a random fluctuation in blackness. The graining frequencies are generally greater than 1 cycle/mm. Usually graining defects are characterized based on their Noise Power Spectra (NPS). The graining patterns for this research were generated from well documented printer defects. A grain defect was scanned and the result was multiplied by a Gaussian envelope to get rid of the abrupt edge changes. Graining defects were generated in two different envelope sizes. Figure 2.6 shows the resulting graining defect for two different envelope sizes.

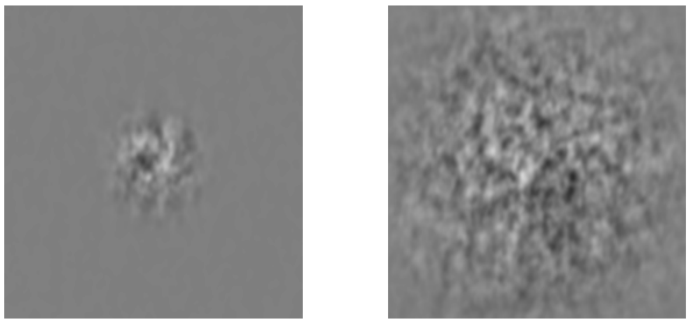

Figure 2.6 Graining Defect Patterns in two various envelope sizes, large and small.

2.1.4 Parametric Scale Variations

The defect patterns as well as the basis functions shown in this section were scaled at different intensity values. The intensity values where determined based on the subject response. That is based on whether the subject can see the pattern or not the intensity value is adjusted. All the patterns where given a maxima amplitude of one. This creates convenience when scaling and gathering analytical data. The contrast for each intensity level was computed as described in chapter 3.

2.2 Presenting to Subjects and Recording Subject Response

Once the stimuli where generated a human subjective test was needed in order to determine the visibility threshold for human observers. The responses of a human population to the stimulus patterns at various contrast levels were used to construct an Empirical Psychometric function. The subjective test presents the stimuli designed with the specifications listed in Section 2.1 of this chapter.

The basis functions results from the subject test are used to obtain the HVS prediction. These predictions are compared to the subject's response from defect patterns testing.

2.2.1 Procedure for taking Subject Test

The purpose of the Subject Test is to estimate the detection threshold for various basis functions (Symlet, Gabor) as well as defect patterns (banding, graining). These threshold results are used to create a prediction algorithm for the perception of print defect patterns. The prediction algorithm is described in details in chapter 3. The prediction algorithm obtained from Symlet and Gabor approach is compared with the results from subjective defect pattern testing. Two alternative forced choice (2AFC) method was used combined with a staircase adaptive procedure. More information about 2AFC and staircase method is provided in Section 2.2.2.

2.2.2 Psychometric Subject Test Setup

The Psychometric subject test was designed following the guidelines shown below.

Design of Psychometric Subject Test:

Psychometric Subject Test was developed at the University of Kentucky, Lexington KY. The test was designed to obtain human responses to visual pattern required to create an Empirical Psychometric Curve. Four classes of patterns where tested, Gabor, Symlets, Banding and Graining. A total of 60 subjects where tested.

Stimuli Display:

The subjects observed the stimuli in form of a movie with 500ms temporal window. The reason for the movie is to avoid image adaptability. The movie was designed using the guidelines from ModelFest. Displaying patterns in form of a movie reduces the effects of visual adaptations to the stimuli. Thirty movie frames were created by generating a Gaussian envelope of 500ms temporal window with unit amplitude. Each of the thirty frames is multiplied to the Gaussian temporal window and to a certain signal scale. The result is added to the background. If S(X, Y, θ) represents the stimuli (X and Y are spatial coordinates, and θ is the orientation) and g (t) is the Gaussian window represented by the equation:

$$g(t) = \frac{1}{\sqrt{2\pi}\sigma} \exp(-\frac{t^2}{2\sigma^2}) \qquad (2.2.1)$$

were t is the temporal window of 500ms for a frame rate of 30 frames per second and σ is the standard deviation, then:

$$M(X,Y,\theta,t) = B + (A * S(X,Y,\theta) * g(t)) \qquad (2.2.2)$$

represents the displayed movie of 500ms temporal window. B represents the background value which was 32cd/m^2, and A represents the signal scale amplitude.

2AFC Method:

The two forced choice method (2AFC) consist of displaying two images to the subject, one image containing just the background and the other containing a scaled stimulus pattern added to the background. The subject has to decide whether he observes the pattern of interest in the first or the second image. The subject can select only one of the two images. If the subject is not sure which image contains the pattern then he/she is forced to make a guess.

Adaptive Staircase Method:

In the adaptive staircase method the magnitude of the stimulus is varied automatically leading to an efficient estimation of the threshold for detection or discrimination. Staircase method assumes that the subject is more likely to make correct decisions for large stimuli magnitudes. The Staircase in our research was designed using an up rule of one and a down-rule of two. That is after two consecutive correct decisions the amplitude scale of the signal is reduced. After the user makes the first wrong decision the increment for adjusting the contrast level is reduce by half. This is known as a downturn. This allows for better resolution near the critical contract region of the psychometric function toward the threshold point of interest. One draw back would be if the subject would make an incorrect decision in the first few trials. To take in account for this the test was designed so that the user would very clearly detect the pattern in the first 5-6 trials. Adaptive staircase controls the strength of the stimuli by changing variable *A* in equation (2.2.2).

Tutorial:

Before taking the subject test a simple tutorial is shown to familiarize the user with the stimuli that will be presented and to teach users how to operate the controls necessary for taking the test. The tutorial session lasts for a 4 minutes and a simple tutorial test is run to ensure that the user is comfortable with using the Psychometric Subject Test. Also a mandatory consent form was presented to the subjects. The consent form would provide the user with information about the test and the testing guidelines. The subjects were selected at random. A close to normal vision was required for all subjects. If the subjects normally wear eye glasses they were required to wear the glasses during the test.

Software used:

The software used to implement the Subject Test was Matlab version 7.0 and the Psychometric Toolbox 2.54.

Seating Conditions:

Seating distance for subjects was set to be 2.43 meters away from the monitor. This distance is set for a resolution of 1150 pixels and a monitor width of 480mm. This corresponds to a pixel size of 0.5 min and for a pattern size of 256x 256. The seating distance (D) for 0.5 min pixel width was computed using equation (2):

$$D = \frac{\frac{(\mathrm{L} * \mathrm{d})}{2R}}{(\tan(\frac{d}{240}) * \frac{\pi}{180}) * 1000} \qquad (2.2.3)$$

where L is the length of the LCD screen in millimeter, R is the screen resolution in pixels, and d is the image size (for our case 256x256). The formula is divided by 1000 to give a distance result in meters.

Controls:

Inputs: Logitech cordless optical mouse with 30 feet communication distance.
Output: Speaker Feedback. Since the subjects were required to seat 2.43 meters away from the monitor the cordless mouse was a optimal choice.

Monitor:

The monitor used is a 20.1 inch Planar 210M with pixel pitch of 0.255mm.

Display viewing rate: 60 Hz. Faster rates are also acceptable.

Maxima viewing angle: 170 degrees.

Display area: 480mm horizontal, 306 mm vertical.

Display mean luminance: +/- 30 cd/m^2

Display Pixel size: The image size will be 256 X 256 pixels.

Viewing conditions:

Binocular viewing: It is required that subjects view the display using both eyes. Also it is expected that subjects have close to normal vision.

Fixation: A black fixation point will be moving around in four corners of the screen. Since the background luminance was 32cd/m^2 and thus the monitor is on the bright side a black fixation point was easier to detect. The pattern was displayed where the fixation point is located. The center of the pattern was aligned to the fixation point. The fixation point and thus the pattern were moved in four corners during the test to avoid visual system adaptation. Adaptation could increase the chance of memory effects. Also it reduces fatigue associated with looking at one spot.

Audio Cues:

Audio Feedback was provided during the Tutorial to explain to the subject the procedures for taking the Psychometric Subject Test.

Also Audio Feedback was used during the subject test. For each correct or incorrect decision an audio feedback was generated to indicate weather the subject decision was correct or not.

Visual Feedback:

Audio Feedback was associated with a visual feedback to indicate whether subject's decision was correct or incorrect.

Estimated Time:

Estimated time varies depending on the levels tested for each subjects. For subject tested on Symlet and Gabor patterns levels 4-6 the estimated time was 15 minutes. For Symlet and Gabor patterns level 2 the estimated time was 3 minutes. For banding defect patterns estimated time was 6 minutes. The subjects were divided into 6 groups with 10 subjects per group. Group 1 was tested on Symlets frequencies of 1.40 and 2.81, group 2 on Symlet frequencies 5.62 11.25 and 22.5. Group 3 and 4 was tested for Gabor patterns of same frequencies. Group 5 was tested on banding patterns and group six on graining defect patterns.

2.2.3 Calibration

For each subject, the amplitude scale A of equation (2.2.2) and the decision process was recorded. For each pattern and orientation, fifteen trials were presented, thus fifteen various signal intensities where recorded as well as fifteen subject decisions. Fifteen trials were selected as the optimal number to obtain the final threshold as well as to reduce the testing time. User decision where recorded as a value 0 or 1, where 0 indicated incorrect decision and one indicated correct decision. The signal scale values and decision values were stored in a .mat file for each individual subject. The signal scale values were stored as buffer values from 0-255. These values were than converted to contrast values as described below. Since it is not possible to obtain 1024 gray scale levels on a 8 bit graphic card the gamma value was adjusted to compensate for the system setbacks. The gamma value was set at 3.5.

Contrast Computations:

First the signal scale values were converted to luminance values by interpolating the buffer values with luminance data measured using Minolta CS-100 chroma meter. Using same lighting conditions as the conditions during subject testing, measurements were taken for a range of buffer values from 0-255 with step increments of 16. For each buffer value the appropriate luminance values in cd/m^2 were measured using the chroma meter. The buffer values vector is [0 16, 32, 48, 64, 80, 96, 112, 128, 144, 160, 176, 192, 208, 224, 240, 255]. This corresponds to a luminance vector measured with chroma meter of

[0.21, 1.93, 5.22, 8.61, 11.9, 15.2, 17.7, 20.5, 22.8, 25.8, 28, 29.5, 32, 34.2, 36, 38.1, 39.5]. A plot of buffer values versus luminance values is shown in figure 2.7.

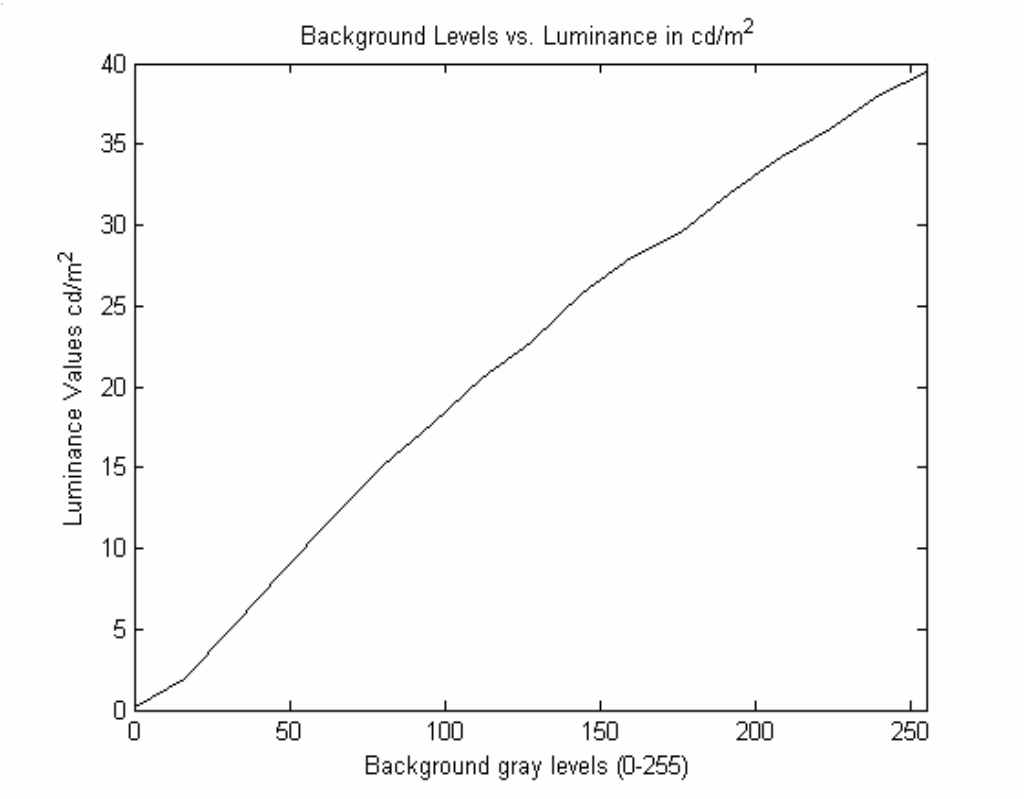

Figure 2.7 Plot of Buffer Values vs. Luminance Values

The background value of the subject test was 192 which correspond to 32 cd/m^2 luminance value. This is within the specified luminance range of Modelfest which requires a background value of 30 +/- 5 cd/m^2. Next a conversion to contrast values was performed. Contrast is a measure of luminance variation relative to luminance in surrounding region. For all the banding defect patterns and basis functions contrast was computed as:

$$C = \frac{\max(M(X,Y,\theta,t)) - \min(M(X,Y,\theta,t))}{B} \qquad (2.2.4)$$

Where B is background luminance value of 32 cd/m^2. Equation (2.2.4) holds true for all patterns except grain patterns. For grain patterns contrast is computed using the formula:

$$C = \frac{\left[\sum_{X,Y}(M(X,Y,\theta,T))\right]^{1/2}}{\pi r^2} \qquad (2.2.5)$$

where r is the area of support for the grain pattern in pixels, so r is the radius, C is the RMS value of the pattern and M is the test pattern in cd/m^2 with the mean/background subtracted out.

A more in depth explanation of contrast computation is described in chapter 3.

2.3 Chapter Summary

In this chapter we introduced the basis functions used to create prediction models of the HVS as well as the defect patterns. The prediction models where Gabor and Symlet basis functions. The defect patterns consisted of banding and graining defects. The experimental setup in this chapter was created using guidelines from ModelFest as indicated in chapter 1. This chapter also introduces the Subjective Testing and also all the guidelines followed to perform the subjective testing.

CHAPTER 3

Prediction Procedure

This chapter discusses the prediction process used to obtain the detection thresholds of the human visual system for print defect patterns. As described in chapter 2, Gabor patterns are well known for predicting the threshold of the visual system, due to the fact that the human visual receptors have Gabor like characteristics. Many researchers are lately looking at Symlets as a new mean of HVS prediction. This topic is covered in details in chapter 1. Symlet based prediction and Gabor based prediction are the two approaches used in this research. The results obtained from each kind of prediction are finally compared to the results obtained from subject testing also known as empirical results.

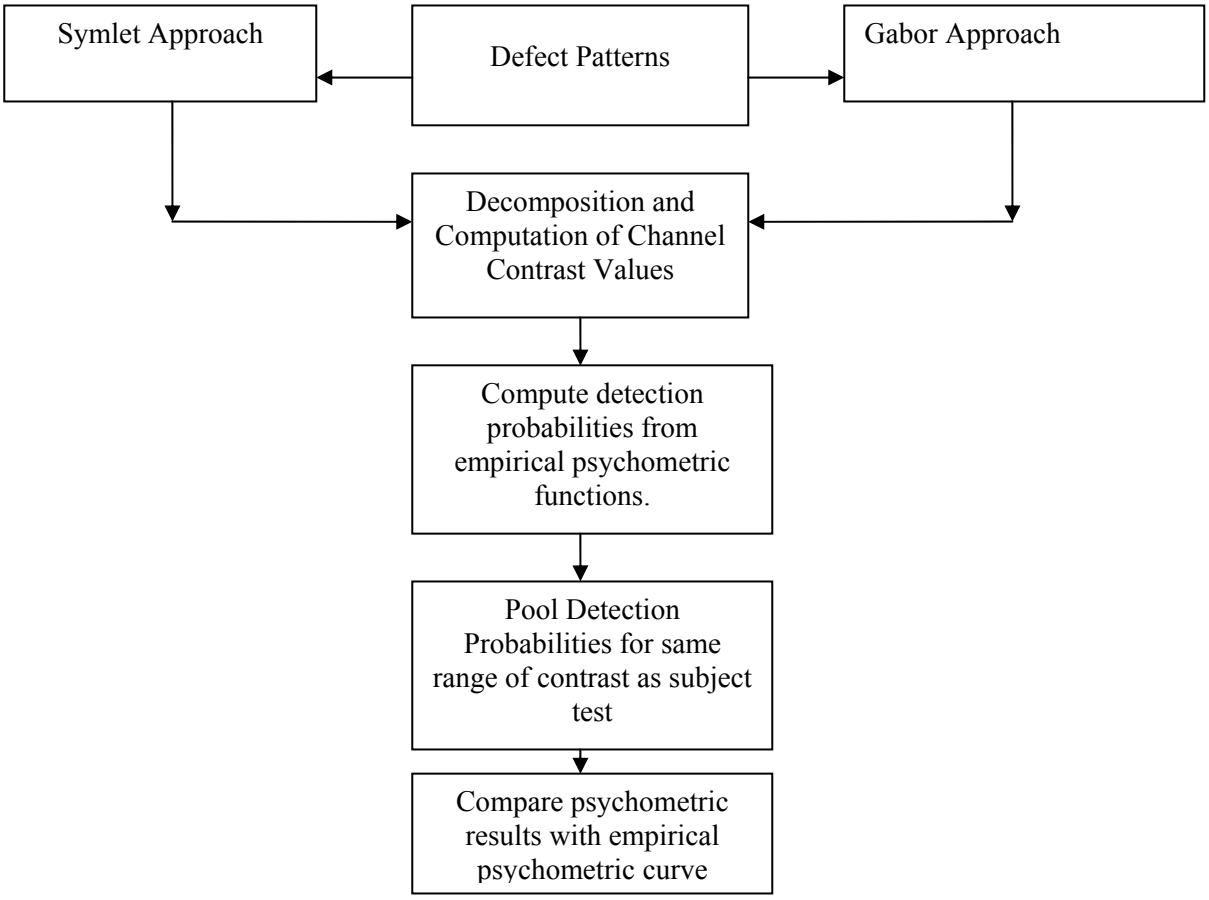

Figure 3.1 Organizational chart describing prediction approaches

The organizational chart shown in Figure 3.1 above represents a map for the remainder of this chapter. This chart illustrates what is known as the pooling process which is a process that determines the detection probabilities of defect patterns at various intensities.

3.1 Defect patterns and basis functions tested

As described in chapter 2, two kinds of defect patterns were tested, banding and graining patterns. The patterns are shown below in figure 3.2.The subjects where tested using these defect patterns following the testing guidelines shown in chapter 2 of the thesis.

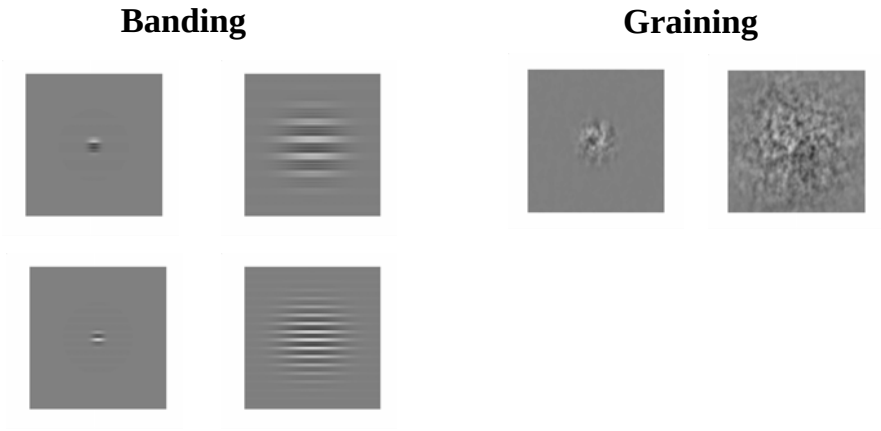

Figure 3.2 Banding and Graining Defect Patterns

For convenience we will refer to the upper left hand corner of the figure 3.2 as banding 1-1. The upper right hand corner will be referred as banding 1-2. This is following an i,j matrix notation. Thus the lower right hand corner would be referred as banding 2-2. Thus as banding 1-1 represents low frequency (4cpd) small envelope banding pattern. Banding 1-2 represents low frequency (4cpd) large envelope banding pattern. Banding 2-1 represents high frequency (8cpd) small envelope banding pattern, and banding 2-2 represents high frequency (8cpd) large envelope banding pattern.

The basis function patterns tested are shown below in figure 3.3. Only the basis function levels 3-6 where tested. Due to limitations in display resolution level 2 (22.5cpd) was dropped from the experiment since subjects could not detect it. The selected frequencies

for the basis functions of figure 3.3 are [1.40, 2.81, 5.62, 11.25, 22.5] cycles/degree (CPD).

Both the Gabor and Symlet patterns are matched in frequency and amplitude. The subjects were tested for three orientations vertical, horizontal and diagonal. More detailed information about the testing procedure is described in chapter 2.

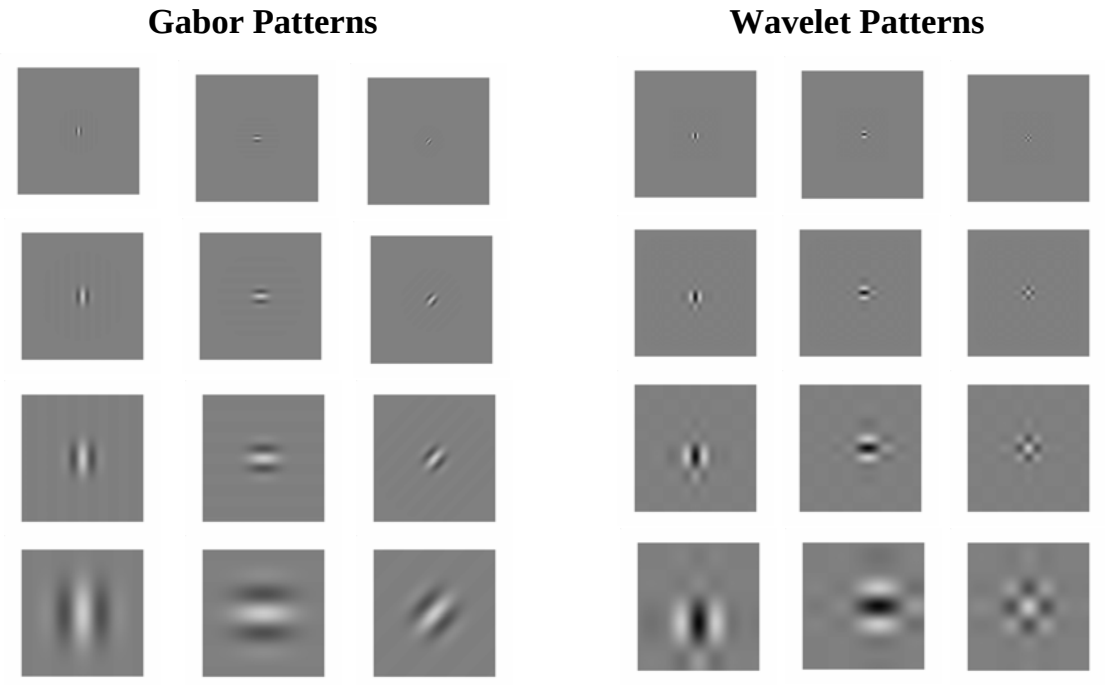

Figure 3.3 Gabor and Symlet basis functions

3.2 Symlet Prediction Approach

This section describes the Symlet prediction approach for obtaining detection probabilities of the human visual system. A new tendency has recently been to describe the HVS model using Symlet approach due to their orthogonal characteristics. Also Symlets can represent defect patterns in fewer coefficients which reduce computational errors. As indicated in chapter 2, the subjects where tested for the Symlet basis patterns shown in figure 3.3. Both their decisions and stimuli intensities for each decision where stored for analysis. An empirical psychometric curve was constructed based on the user's

decision. The sections that follow explain in more details what the psychometric curve is and what are the benefits of using the psychometric curve.

3.2.1 Psychometric Curves

This section provides an introduction to the psychometric curves and their importance in representing the response of the visual system.

Psychometric function (PF) is defined as a measure relating probability of subject's response to the physical measure of stimulus such as intensity. The abscissa of PF is the stimulus strength while the ordinate is the probability of observer's response. When expressed as a function of log intensity, most previous works assumed, the shape of psychometric function remains the same for all conditions.

This property of the psychometric function allows us to describe any psychometric function $p_T(x)$ in terms of canonical form $\psi(x)$ by the relation

$$p_T(x) = \Psi(x - T) \qquad (3.2.1)$$

where T is the detection threshold, which can have any particular value.

This psychometric function where used by Watson and Pelli [19].

3.2.2 Weibull Psychometric Curve

As described by Watson and Pelli the Weibull psychometric curve has the form:

$$w(c;T,\beta,\gamma) = 1 + (1-\gamma)\exp(-10^{(\beta/20)(c-T+\varepsilon)}) \qquad (3.2.2)$$

Parameter c in Equation (3.2.2) represents the contrast values in decibels. The parameter γ represents the patterns detection probability at zero intensity. For the 2AFC test used in this research the value of γ is set to 0.5 because the subject is forced two choose one of two possible choices. The number of alternative choices is presented by $1/\gamma$. From literature the value of β is set at 3.5 and T is defined as the 70.7% correct threshold point for 2AFC method [19]. Varying β and T will alter the shape of the psychometric curve. Figure 1 shows Weibull psychometric curve constructed with set β=3.5 and varying threshold T -4db, 0db and 4 db.

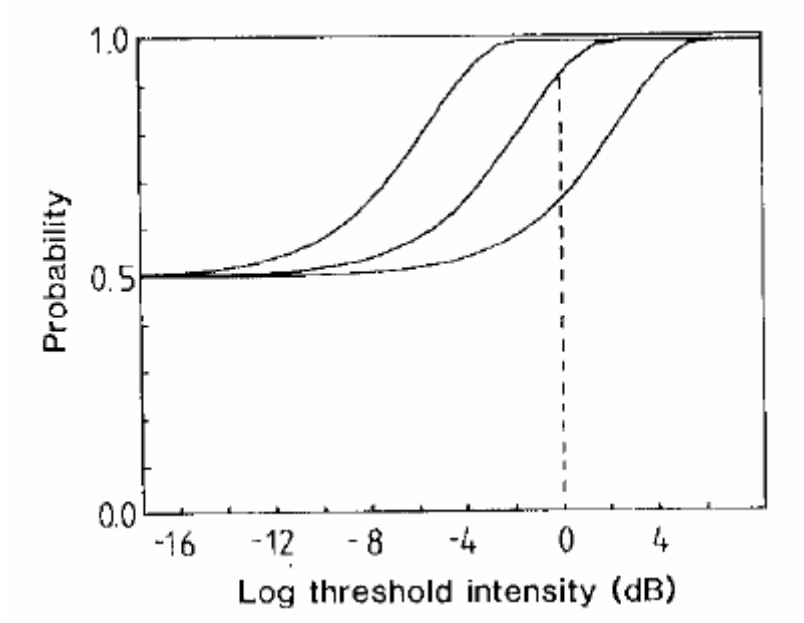

Figure 3.4 Psychometric curves, β=3.5 and T values, -4db, 0, 4db adapted from [19].

Varying the threshold T will shift the psychometric curve along the x axis as shown in figure 3.4. Varying β will affect the slope of the psychometric curve.

Since 2AFC test is used the lowest possible detection probability would be 50%. This represents the case when subjects are not sure whether they observe the pattern of interest, and thus they are forced to guess. When the subject is guessing the probability of guessing correct is 50%. The 100% probability represents the full confidence point where the subjects are 100% sure they observe the pattern of interest. In our experiment the patterns are clearly visible by general population in the first few trials of the test, indicating a detection probability of 100%. When the pattern does not exceed the visual threshold, the subject is forced to guess resulting in a detection probability of 50%.

Lets define random variable S_D as the event that HVS correctly detects the pattern at the given contrast level c among the $1/\gamma$ alternative patterns, where γ is set at 0.5 for the 2AFC method used in this experiment. Then an alternative form of representing equation 3.2.2 would be:

$$W(c;T,\beta,\gamma) = P\{S_D|c\} \qquad (3.2.2a)$$

Previous research sets the β value of equation 3.2.2 to 3.5 [16]. The Weibull curve is than determined by taking the subjects contrast value at the convergence probability level. In his previous work Venkatesh determined the threshold as the contrast at the last trial taken by the subjects. For example if the subject observed a particular pattern for 15 trials the threshold was based on the subject response to the 15^{th} trial. After a bootstrapping process described below the median of all the thresholds from all subjects was inserted in equation 3.2.2 with the value of β set at 3.5.

This method of computing the psychometric curve was used by Venkatesh in his thesis "Wavelet and Sine based analysis of Print Quality evaluations"[16]. In his research Venkatesh constructed the Weibull psychometric curve by setting the Beta value to 3.5, which will yield threshold intensities with .92 probability of success. In his research Venkatesh used bootstrapping to estimate the 92% threshold. Bootstrapping is a re-sampling technique that assumes that the observations are independent and performs sampling with replacement from the acquired data where each observation has the same probability of being chosen each time. In a pool of n values, bootstrapping consist of picking a random value out of the pool of n values, placing the chosen value back on the pool after each pick. This procedure is then repeated k times. This ensures independent bootstrap samples. In his research for each stimuli Venkatesh collected the threshold data for different subjects. The bootstrap sample was created by picking values from this pool of threshold data 64 times with replacement.

Next he computed the median of his bootstrap sample. The median was taken as the final threshold and it was plugged into the Weibull psychometric function with the value of Beta set at 3.5. Both sinusoid and Symlet prediction psychometric curves were constructed using this approach. For our experiment since we used a 2AFC method convergence probability is 70.7%.

The approach used in this thesis is different from Venkatesh approach. Instead of using only the threshold point to construct the basis function psychometric curves, in this research we constructed the curves taking into account all the subject responses for different contrast values, not just the threshold value. Thus all the subject response for different intensities for a particular stimulus was taken into account. Next the resulting

curve from the data was best fitted to the Weibull psychometric curve. The values of β and T where adjusted until the Mean Square Error between the subject data values and Weibull distribution was minimized. This approach is presented in more details as follows.

3.2.3 Derivation of Empirical Psychometric Curve

The psychometric curves obtained from subject testing data as explained in chapter two will be referred to as Empirical Psychometric curves.

For each basis stimuli (Figure 3.3) the subject's response and contrast values were recorded for 15 trials. All the contrast values from all subject data where stored in a vector and sorted in an increasing order. Next step was to group these contrast values on different bins based on a set sampling rate. A histogram of correct decisions over ranges or bins of stimuli contrast from all subject responses was constructed. Number of correct and incorrect decisions was recorded for each bin of contrast values.

The decision probability in each contrast bin was computed as:

$$\overline{F_e}(c;T,\beta,\gamma) = P_D = \frac{N_C(c)}{N_T(c)} \qquad (3.2.3)$$

where N_C represents the number of correct decision for a particular contrast bin, and N_T represents total number of decisions (correct and incorrect) obtained from this pool of subjects for the corresponding bin. $\overline{F_e}(c;T,\beta,\gamma)$ represents the resulting empirical psychometric curve obtained from testing human subjects. The contrast value *c* represents the contrast value for the center of each bin. The number of bins picked was determined by looking at the resulting shape of the psychometric curve. This is different from Venkantesh's method, since we are using a staircase method which allows us to pick from a wide range of contrast values not jus the threshold contrast.

Next a plot of the empirical psychometric function was obtain by plotting the contrast bins in the x axis and probabilities of correct decision for each particular contrast bin in the y axis.

The Weibull psychometric curve was fitted to the empirical curve obtained from subject test. In the Weibull function (3.2.2) by adjusting the values of T and β the best fit to the empirical psychometric curve was obtained. This fit minimizes the Mean Squared Error (MSE).

Mean Square Error is defined as the average of the square of the difference between the desired response and the actual system output (the error). If $F_e(c)$ represents the psychometric curve obtained from the subject data as a function of contrast, and W represents the Weibull psychometric curve of equation 3.2.2 then the mean square error of the curves is found using the formula:

$$MSE\ (c;T,\beta) = \frac{\sum (\overline{F_e}(c) - W(c;T,\beta,\gamma))^2}{k} \qquad (3.2.4)$$

In equation 3.2.4 k represents the number of bins of contrast axis. The value of γ is set at 0.5 for 2AFC method. The best fit values (smallest MSE) of β and T are recorded for each channel. Out of many possible $W(c;T,\beta,\gamma)$ curves constructed as for different values of T and β, $\overline{W}(c;T,\beta,\gamma)$ represents the best fit (smallest MSE) to the subjective data psychometric curve. This method is different from various research work where T was estimated and Beta was set to constant. In our research we varied both T and β to obtain $\overline{W}(c;T,\beta,\gamma)$ which represents the best fit to the subject data psychometric curve $\overline{F_e}(c;T,\beta,\gamma)$.

Once the best fit of both curves (Weibull and Empirical Psychometric curve) was obtained, the Weibull curve was adjusted to provide probability values from zero to one with convergence probability point at 70.7%. This was done by modifying equation 3.2.2.

$$w_T(c,T,\beta,\gamma) = 1 + \exp(-10^{(\beta\min/20)(c-T\min+\varepsilon)}) \qquad (3.2.5)$$

The value of γ in equation 3.2.2 was set at zero resulting in equation 3.2.5. This would adjust the curve shown in equation 3.2.5 to contain probability values from zero to one. As described earlier the value of 1/γ represents the number of alternative patterns shown to the subject. Thus as $\gamma \to 0$ then $\frac{1}{\gamma} \to \infty$ which means we have infinite number of

alternative patterns, representing the human response when looking at a single pattern (probability of detection goes to zero when pattern is not visible).

Equation 3.2.5 was solved for ε at the .707 convergence probability point where the values of β_{min} and T_{min} are known. β_{min} and T_{min} represent the value of β and T that minimizes the mean square error. The reason for adjusting the empirical psychometric curve is to obtain values ranging from zero to one. As described in later in section 3.3 pooling consists of multiplying the probability values of all channels and subtracting one from the result [16]. Thus if our lowest probability is 0.5 we would never achieve a zero probability using pooling method.

3.2.4 Psychometric Results

The psychometric results for banding defect patterns are shown below in figure 3.5. The dotted line represents the Weibull Psychometric function constructed using equation (3.2.2). The dashed line represents psychometric curve obtained directly from subject testing. The dotted and dashed curves are fitted to provide smallest MSE. The values of β and T that minimize the MSE were recorded. The solid black line represents the resulting empirical psychometric curve with a probability range from 0 to1.

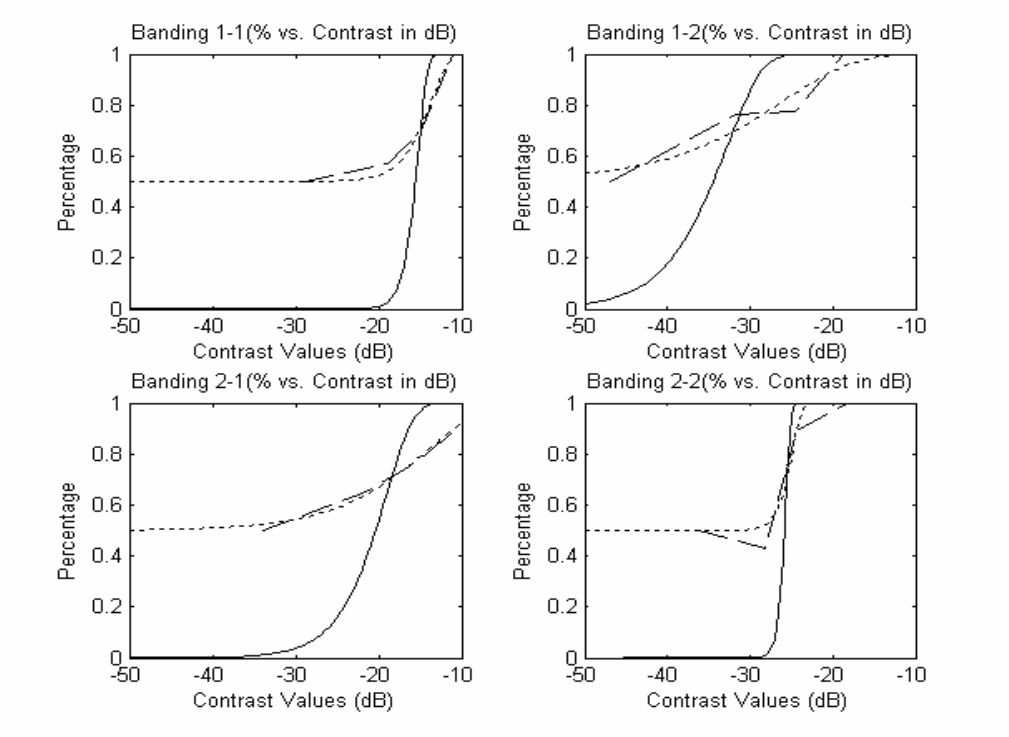

Figure 3.5 Empirical Psychometric Results for Banding Defect patterns.

In Figure 3.5 the dashed line represents the subjective data, the dotted line represents the Weibull best fit to the subjective data and the solid line represents the Weibull stretched from 0-1 where the convergence probability 70.7% point is the same as the Weibull curve (dotted line).

The empirical psychometric curves were constructed for both the basis functions as well as defect patterns. Figure 3.5 shows the empirical psychometric results for the banding defect patterns only.

3.3 Decomposition and Computation of Channel Contrast Values

In order to mimic the receptive filters of the visual channels an observed pattern is decomposed with the basis functions. The Gabor and Symlet basis functions represent the receptive filters of the visual cortex.

3.3.1 Decomposition

Same defect patterns that the subjects observed during the test are decomposed with the Symlet coefficients. The defect patterns have values in cd/m^2. This insures display independent metrics. The convergence of the defect patterns into candelas values is obtained by interpolating with the curve shown in figure 3.6. This curve was obtained by setting the monitor gamma and measuring the light intensity with a chromameter for different gray scales. The x axis of the figure indicates LCD screen buffer values from 0-255 and the y axis consist of luminance values in cd/m^2.

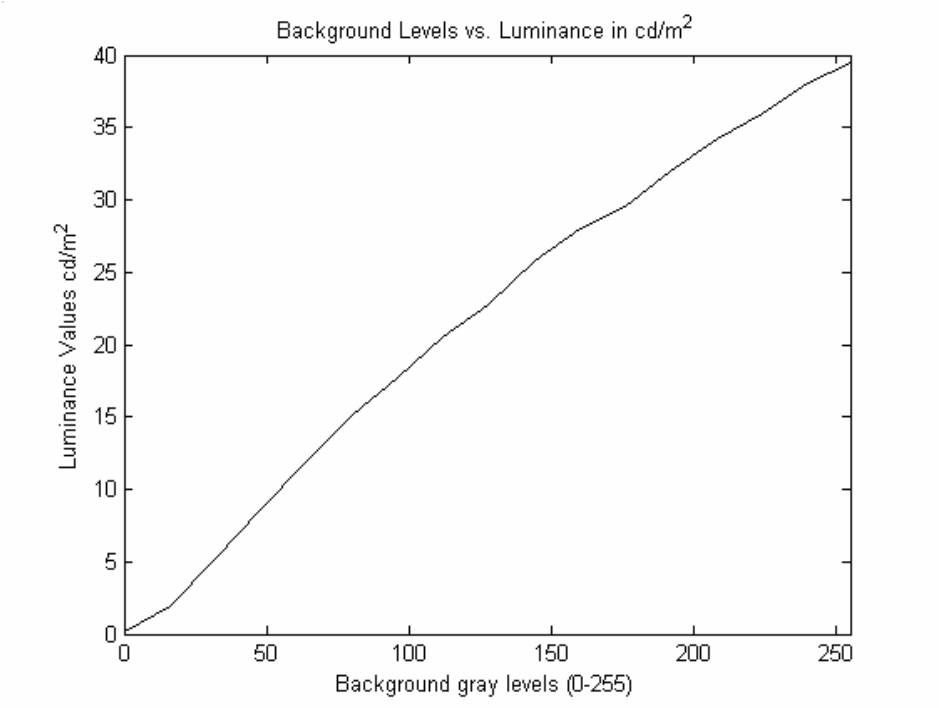

Figure 3.6 Buffer Values vs. Luminance Values

Each resulting banding defect pattern of figure 3.2 was convolved with each Symlet channel shown in figure 3.3. Figure 3.7 illustrates this process.

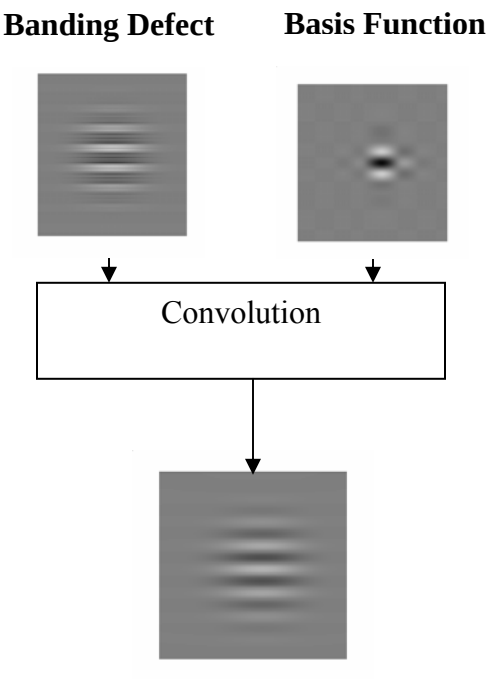

Figure 3.7 Decomposition Process for banding defect patterns

The Symlet coefficients were obtained using the up sampling method explained in details in chapter 2. This decomposition method is analogous to the decomposition that the visual system performs into independent spatial channels when a defect pattern is observed.

3.3.2 Computation of Contrast Values

Defect patterns contain a absolute maxima as well as local maximas. One question arises. Does the HVS consider one maxima or multiple maximas in order to perform threshold estimations. Thus we designed our experiment to be able to select one or more uncorrelated maximas from each channel. For each decomposition channel obtained in step 3, N independent maximas where chosen, an absolute maxima and local maximas. Since the Symlet and Gabor coefficients where generated without down sampling, the adjacent samples for the low-pass level are highly correlated. The contrast for these N maximas was computed and the resulting probability values where obtained by interpolating with the empirical psychometric curve. Depending on the level of decomposition the absolute maxima was first determined. The surrounding pixels within

$2^{(\text{level}-1)}$ of the absolute maxima were zeroed out. For example for a level 2 coefficients we would zero out the maxima and all the pixels within 2 pixels of the absolute maxima and so forth. This process was repeated to obtain N independent maximas per channel. The independent maximas were converted into contrast values by dividing by the DC bias value which was the background value for our experiment.

Let $C_{jk}(i)$ be the channel contrast with subscript i representing the i^{th} largest coefficient. All the absolute values of coefficients are ordered in the channel from the largest to smallest $[C_{(1)},C_{(2)},C_{(3)}\ldots C_{(N)}]$. Then the detection probability in a particular channel was computed as:

$$P_{jk} = \prod_{i=1}^{N} P\{C_{jk}(i)\} \qquad (3.3.1)$$

The terms j,k represent the particular decomposition channel, $C_{jk}(i)$ represents the i^{th} largest independent coefficient selected in the channel. Each resulting contrast was interpolated with the empirical psychometric curve for the particular basis function in order to obtain a probability value associated with the particular contrast. Thus from equation 3.3.1 we notice that we can either pick one maxima value or multiple uncorrelated maximas. In chapter four we will determine which is the optimal number of maximas we should pick from each channel in order to better predict the HVS response to the defect patterns.

3.3.3 Computing detection probabilities from the Empirical Curves

The final step consisted of pooling the probability values from the empirical psychometric curves. The probability pooling was performed for each contrast value in equation (3.3.1) assuming that all the contrast values represented independent visual channels. Detection probability is computed by finding the probability of not detecting the basis function in any of the 12 channels and subtracting the result from unity.

$$P_d = 1 - \prod_{j=1}^{J}\prod_{k=1}^{K}(1 - P_{jk}) \qquad (3.3.2)$$

The terms j,k represent the decomposition channels, For each channel the probability associated with the maxima contrast of that channel was obtained from the Empirical Psychometric function of the Symlet basis patterns described in section 3.3.2. In equation 3.3.2 the terms $(1-P_{jk})$ represents the probability that the defect is not detected in a particular channel. Thus we are saying that the HVS does not detect the defect in any of the channels. Then $1-\prod_{j=1}^{J}\prod_{k=1}^{K}(1-P_{jk})$ indicates that the HVS is observing the defect on at least one channel. The same approach was repeated for different intensities. Thus a complete psychometric curve was obtained for various intensity values. The results from these series of curves are shown in chapter 4.

3.4 Gabor Prediction Approach

The Gabor Decomposition approach was similar to the Symlet Decomposition approach. Same procedure described in section 3.3 is used for the Gabor patterns. Same identical approach was used for both Symlet Decomposition and Gabor Decomposition. Please refer to the Symlet Decomposition approach for more detailed information.

3.5 Chapter Summary

This chapter discussed how to obtain an HVS model based on the subject test data. Also the pooling procedure was included in order to obtain the prediction probabilities. The results are shown in chapter 4.

CHAPTER 4

Experimental Results

This chapter presents the experimental results of this thesis. There are two types of prediction results obtained in this test, Gabor approach prediction and Symlet approach prediction. Both types of prediction are compared with empirical results from direct subject testing on the same banding and graining defect patterns. This chapter presents the prediction results for characteristics defect patterns and compares them to results from subject responses tested with the same patterns.

4.1 Experimental Results for Banding Defect Patterns

The methodology described in chapter 3 was used to predict the human visual system response to banding defect patterns. As explained in chapter 3 the banding patterns shown in figure 3.2 where decomposed using Gabor and Symlet decomposition. This resulted in two types of predictions known as Symlet approach prediction and Gabor approach prediction. As indicated in chapter 3, banding 1-1 refers to low frequency (4cpd) small envelope banding pattern, banding 1-2 refers to a low frequency(4cpd) large envelope banding pattern, banding 2-1 refers to a high frequency (8cpd) small envelope banding pattern, and banding 2-2 refers to a high frequency(8cpd) large envelope pattern. Both the banding and graining results are shown in this chapter.

Two versions of the performance metrics were computed after bootstrapping with replacement. These were the mean and standard deviations of the psychometric curves over the bootstrap trials, and the median and inter-quartile distances of the psychometric curves over the bootstrap trials. The comparison between mean and median results will indicate the degree to which outliers existed in the data, whereas the median may converge more slowly to the true underlying value, it is more resistant (ie.. less influenced) to outliers, which are most likely choices where the subjects made mistakes during the test. If results between the 2 versions are similar, the mean value is likely

more accurate. If the results are very different, then outliers had a significant influence and the median results are likely more accurate.

The mean results were computed as follows:

Let vector N= $\{N_1, N_2 \ldots\ldots N_m\}$ represent m subjects that took the test for a particular defect pattern. Out of this pool of subject's, a set of m subjects were randomly picked with replacement for each trial. The psychometric curve W_i was computed for each trial or selection. The process was repeated n times. The mean was computed as:

$$\overline{M} = \frac{\sum_{i=1}^{n} \overline{W_i}}{n} \qquad (4.1.1)$$

where *M* represents the resulting psychometric function computed using the mean of the bootstrap trials and *n* is the total number of bootstrapped trials. For our experiment 20 bootstrapped runs where performed. The standard deviation (STD) of all the bootstrapped sets was also computed. The STD was computed on a non-standard way. We selected all the values below the mean and computed the RMS for the negative STD and also we selected all the values above the mean and computed the RMS for the positive STD. The median was computed in a similar manner to the mean, where the subjects where picked at random with replacement from a pool of *m* subjects. The psychometric results where computed over n bootstrap trials.

Let *N(r : n)* represent the sample with r^{th} magnitude out of n samples, where n represents the number of bootstrapping runs, which is 20 for our experiment. The median *N (10:20)* represent the middle value out of the 20 bootstrapped runs (in the case of an even number the 2 middle samples N(10:20) and N(11:20) were averaged together). The lower quartile value is *N (5:20)* and the upper quartile value is *N (15:20)*. The inter-quartile distance is the difference between these 2 numbers and is analogous to the standard deviation. Because of the exclusion of extreme values, the median typically results in better estimates than the mean in the presence of outliers.

Before we introduce the results lets first identify the metrics used in these results. There are three types of curves shown in the sections that follow. There is a Gabor prediction curve, a Symlet prediction curve and a psychometric curve (subjective curve) obtained from subject data. Both the Gabor and Symlet curves predict or estimate the subject population response to the defect pattern. Within the standard deviation bars of the subject data psychometric curve represents target for the prediction tests. The response corresponding to the .707 probability level will be considered the true subject response and used in the error metric computations. The goal is to better understand how well the prediction follows the subjective data, as well as which prediction approach gives better and more consistent results.

In the figures that follow the solid line represents the defect pattern empirical results from human subject testing. The dashed line represents the Symlet approach prediction and the dotted line represents the Gabor approach prediction. The error bars represent either the standard deviation or inter-quartile distances from the subject data psychometric curve after 20 bootstrapped runs.

4.1.1 Banding results using bootstrapping mean

The results for banding 1-1 which represents a low frequency small envelope defect pattern, are shown below in figure 4.1. These results where obtained by bootstrapping with replacement and computing the mean of all the bootstrapped psychometric sets as indicated in section 4.1. The prediction results are obtained by decomposing the image with the basis functions and picking the absolute maxima from each resulting channel. The probabilities are computed for every contrast maxima in each channel, and the results from all channels are pooled to obtain a probability value. The method is repeated for different contrast values as explained in section 3.3.

In this section the pooling is based on the HVS detecting only one absolute maxima spatially when observing a defect pattern. As shown in equation 4.1.1, in the case of banding defects, the mean of 20 bootstrapped runs was computed, where each run consisted of 8 subjects picked randomly with replacement. As it can be observed from the

figure both the Gabor (dotted line) and Symlet (dashed line) approaches are predicting closely the subjective psychometric data shown with the solid line. The standard deviation (error bars) are also computed from the subjective data. Since we are not dropping subjects form the computations, outliers are averaged in the mean.
From figure 4.1 we notice that both the Gabor and Symlet approach (dotted and dashed line) predicted that the subject should have observed the defect pattern at a lower contrast value than they actually did (solid line).

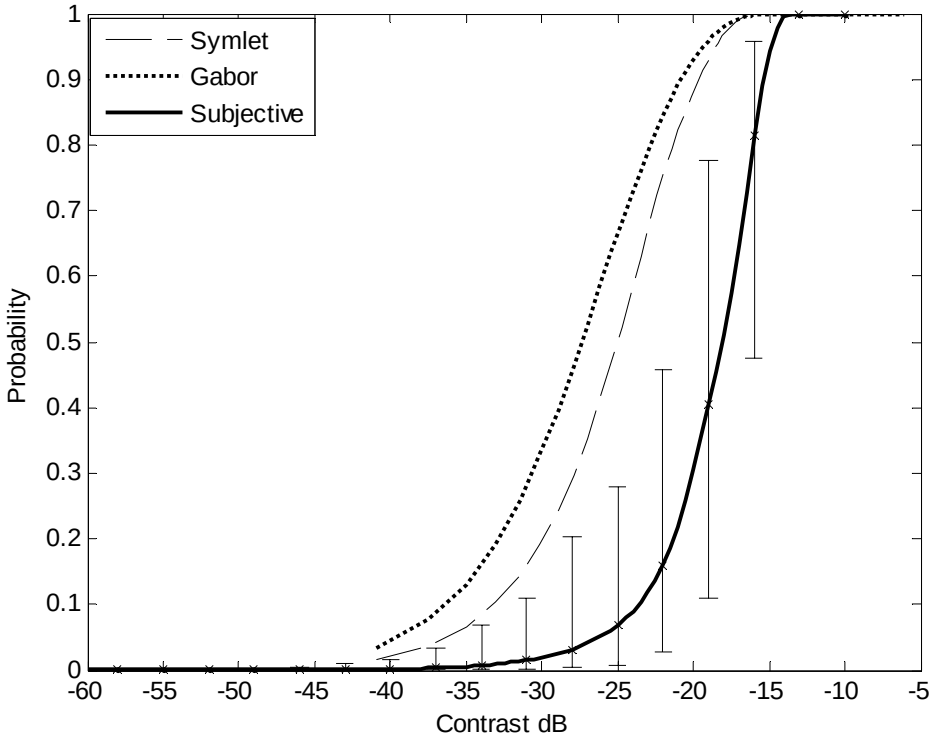

Figure 4.1 Banding 1-1 using bootstrapping mean, low frequency small envelope banding pattern. Assumption is made that HVS detects only the absolute maxima when observing a defect pattern.

Figure 4.2 shows the results for banding 1-2, low frequency large envelope pattern. From this figure we observe that the Symlet pattern is following the empirical data closer than the Gabor pattern. For the case of the Symlets the user is seeing the printing defect at a lower contrast than predicted by Symlet approach. On the other hand the Gabor prediction indicates that the subjects should have observed the pattern at a lower contrast

value. Also, the error bars are longer on the right side of the subjective curve indicating some outliers averaged in the subjective results.

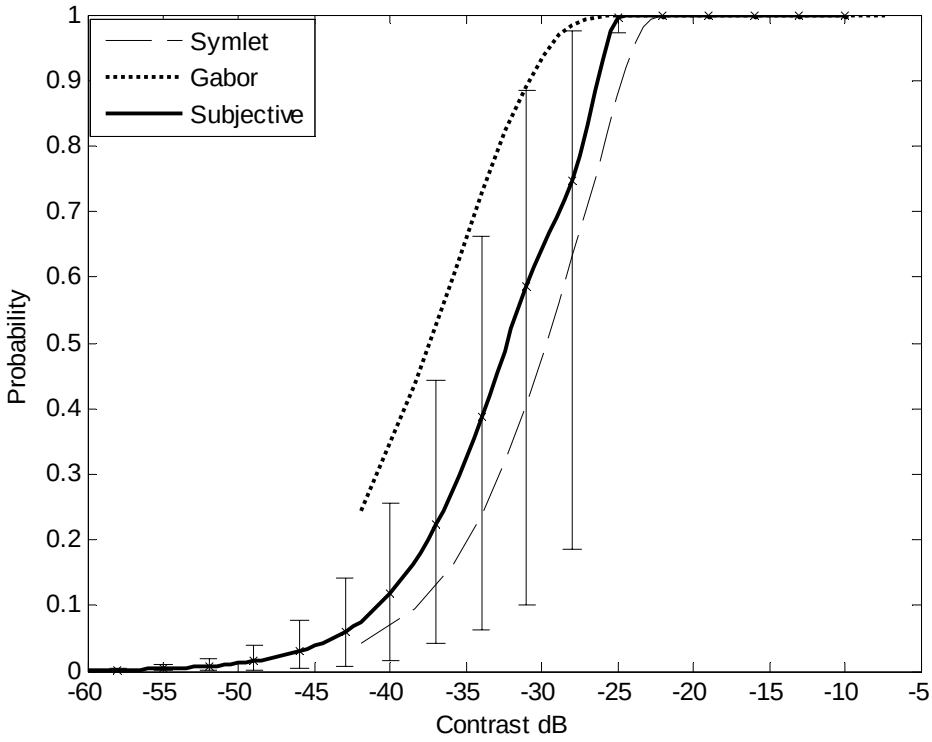

Figure 4.2 Banding 1-2 using bootstrapping mean, low frequency, large envelope banding pattern. Assumption is made that HVS detects only the absolute maxima when observing a defect pattern

Figure 4.3 shows the prediction results for banding pattern 2-1 located in the bottom left hand corner of figure 3.2. This represents the high frequency, small envelope banding pattern.

As it can be observed from the figure both the Gabor prediction is indicating that the defect pattern should have been observed at a higher contrast value than it actually did. The Symlet is outperforming the Gabor approach for this particular defect pattern. The Symlet is predicting pretty close to the convergence probability .707 point.

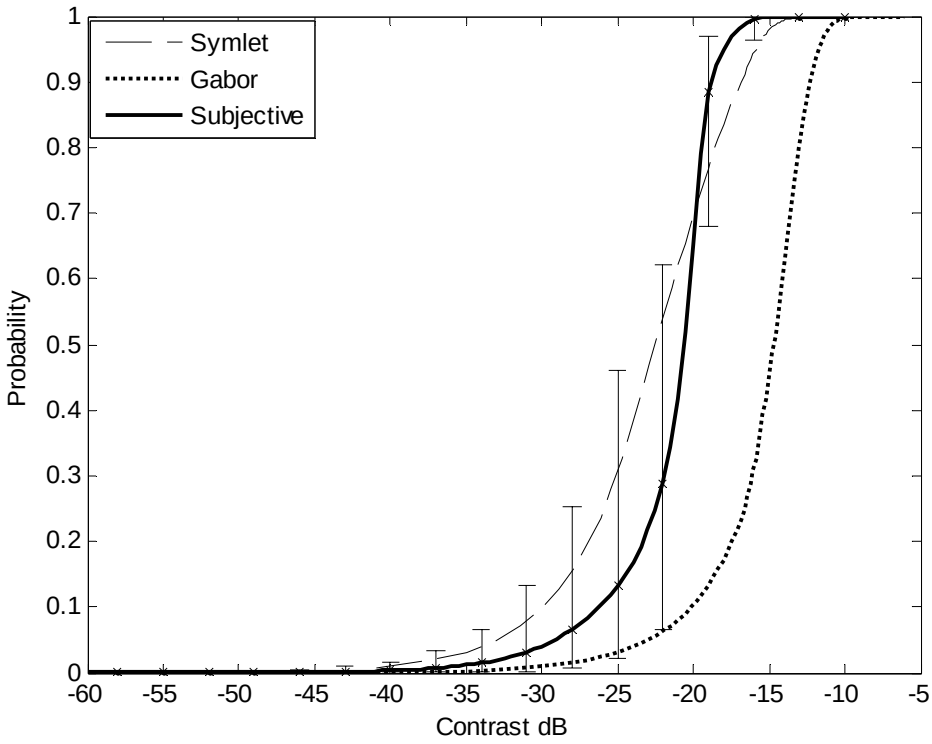

Figure 4.3 Banding 2-1 using bootstrapping mean, high frequency, small envelope banding pattern. Assumption is made that HVS detects only the absolute maxima when observing a defect pattern

Figure 4.4 shows the results from banding 2-2, which represents a high frequency large envelope pattern. In this figure both the Symlet and Gabor predictions are indicating that the subjects should have detected the defect at a higher contrast value.

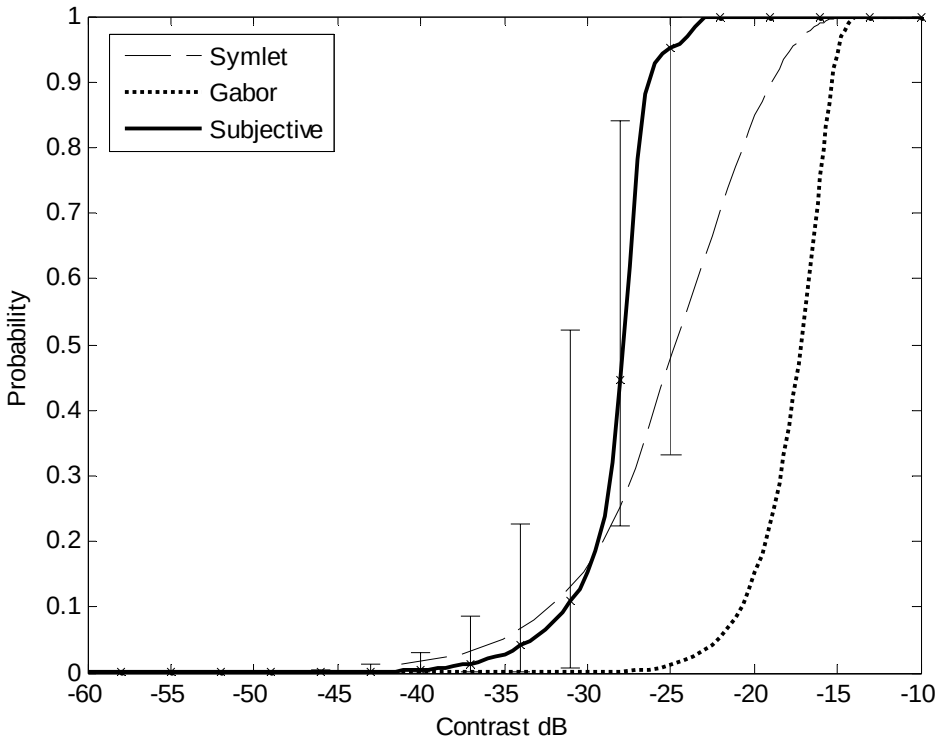

Figure 4. 4 Banding 2-2 using bootstrapping mean, high frequency, large envelope banding pattern. Assumption is made that HVS detects only the absolute maxima when observing a defect pattern

The tabular results taken from figures 4.1 thru 4.4 are shown below in table 4.1. The values in parenthesis indicate the deviance in dB of the prediction to the banding subject test data at the convergence 70.7% probability point. A positive value indicates that we are under predicting while a negative value indicates that we are over predicting.

Table 4.1 Banding defect prediction results at the 70.7 % convergence probability with one maxima picked using the mean. The error between subjective data and prediction is shown in parenthesis.

	Subjective(dB)	Symlet(dB)	Gabor(dB)
Banding 1-1 4cpd, small envelope	-16.62	-22.57(5.94)	-24.33(7.70)
Banding 1-2 4cpd, large envelope	-28.71	-27.03(-1.67)	-34.31(5.60)
Banding 2-1 8cpd, small envelope	-19.8	-19.85(0.05)	-13.54(-6.26)
Banding 2-2 8cpd, large envelope	-27.22	-21.99(-5.23)	-16.19(-11.03)
Error Mean(dB)		-0.22	-0.99
Error STD		4.66	9.08

From the error mean results we notice that the Symlet is performing better than the Gabor even though the difference between the two is minor. The deviation from the empirical data for Symlet in dB is smaller than the deviation of Gabor data. Thus the Gabor prediction is more influenced from outliers than the Symlet prediction. This support the case that the Symlets outperform Gabor patterns since they require fewer coefficients to cover the defect patterns.

4.1.2 Banding results using bootstrapping median

Figures 4.5 thru 4.8 show the results obtained using the median of the subjective results as discussed in section 4.1. Thus the standard deviation error bars look different from the mean results. Overall the median case error bars are more centered to the subjective curve than in the case of the mean. This indicates that the outliers or deviant samples were cases where subjects may missed easily detectable targets, therefore pushing the psychometric curve to a higher threshold values. The median considers the inter-quartile region, thus excluding outliers that fall outside this range. The assumption is made in these results that the HVS detects only the absolute maxima of the defect patterns. In section 4.3 we will try to determine if we require one maxima per spatial channel or multiple uncorrelated maximas.

Figure 4.5 thru 4.8 show an overall improvement of Gabor results when compared to figures 4.1 thru 4.4. This is due to the fact that some of the deviant samples are excluded for the case of the median computation thus reducing the standard deviation of both the Gabor and Symlet predictions. In figure 4.5 the prediction is indicating that the subjects should have detected the defect at a lower contrast than they actually did.

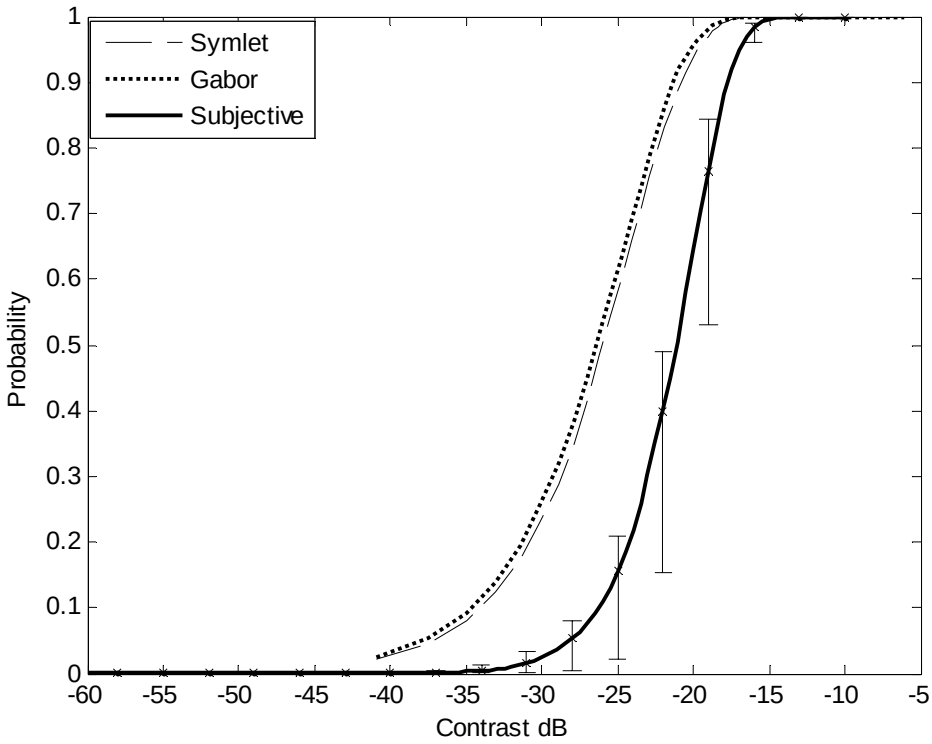

Figure 4.5 Banding 1-1 using bootstrapping median, low frequency, small envelope banding pattern. Assumption is made that HVS detects only the absolute maxima when observing a defect pattern.

In figure 4.6 the Gabor prediction is implying that the defect pattern should have been observed on a weaker state while the Symlet is closely following the actual subjective data (solid line). The Symlet is closely predicting the detection threshold in the neighborhood of the convergence probability point.

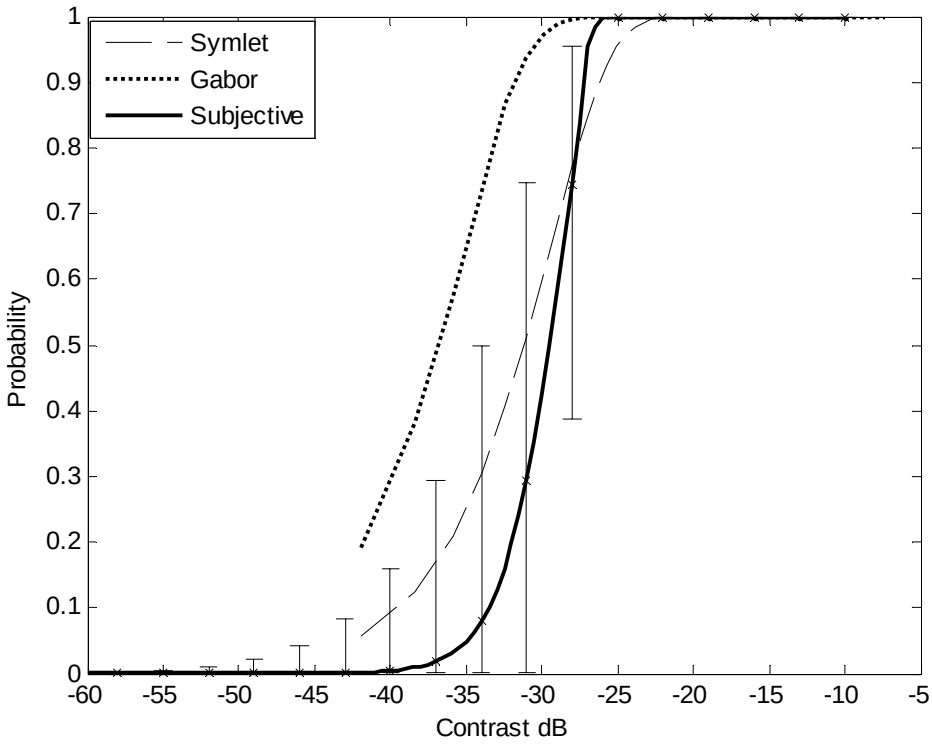

Figure 4.6 Banding 1-2 using bootstrapping median, low frequency, large envelope banding pattern. Assumption is made that HVS detects only the absolute maxima when observing a defect pattern.

In figure 4.7 the Gabor prediction is indicating that the subjects should have detected the defect earlier (higher contrast value) than they actually did. The Symlet prediction is still performing very well around the convergence probability point.

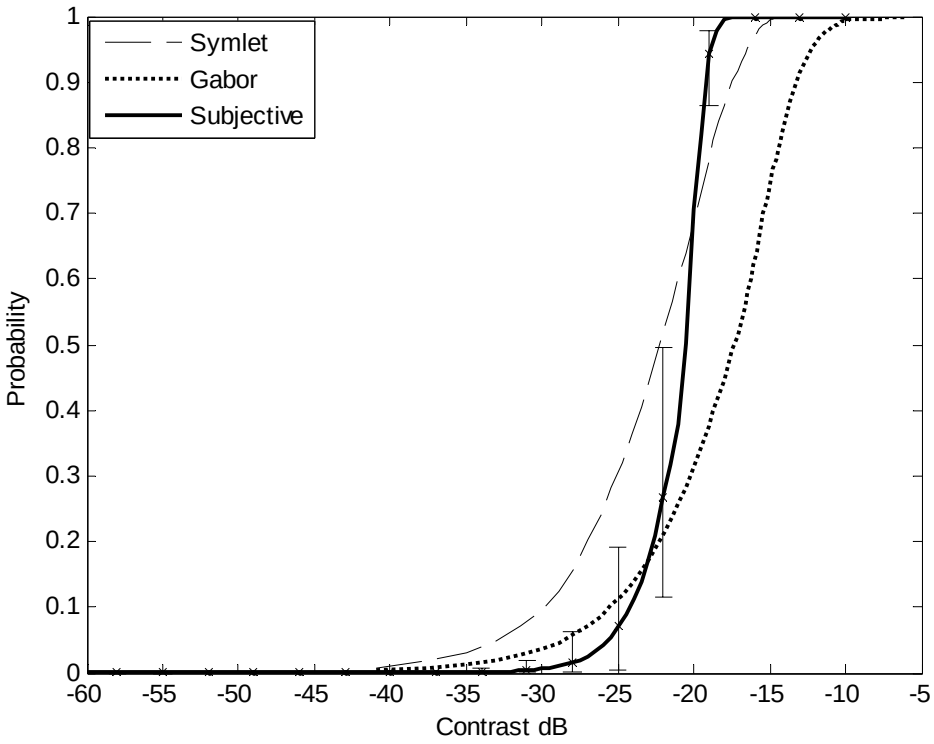

Figure 4.7 Banding 2-1 using bootstrapping median, high frequency, small envelope banding pattern. Assumption is made that HVS detects only the absolute maxima when observing a defect pattern.

In figure 4.8 both prediction approaches are indicating that the defect should have been observed at a higher contrast value.

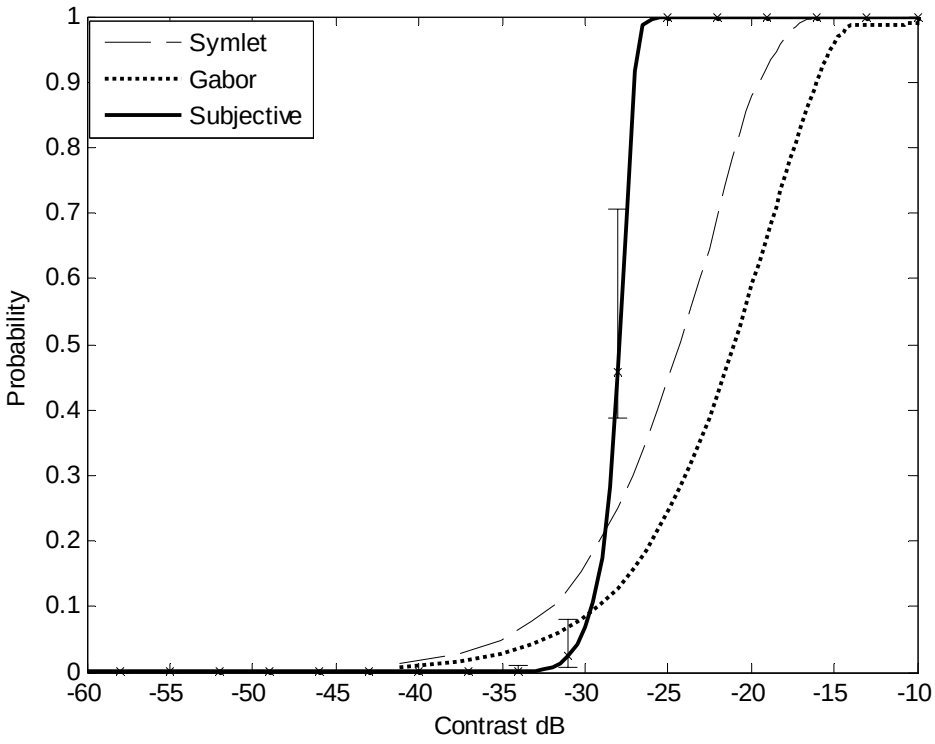

Figure 4.8 Banding 2-2 using bootstrapping median, high frequency, large envelope banding pattern. Assumption is made that HVS detects only the absolute maxima when observing a defect pattern.

Table 4.2 Banding defect prediction results at the 70.7 % convergence probability with one maxima picked for the case of the median. The error between subjective data and prediction is shown in parenthesis.

	Subjective(dB)	Symlet(dB)	Gabor(dB)
Banding 1-1 4cpd, small envelope	-19.50	-23.49(3.99)	-23.88(4.38)
Banding 1-2 4cpd, large envelope	-28.23	-28.74(0.51)	-34.32(6.09)
Banding 2-1 8cpd, small envelope	-20.00	-19.77(-0.22)	-15.32(-4.67)
Banding 2-2 8cpd, large envelope	-27.5	-21.92(-5.57)	-18.56(-8.93)
Error Mean		-0.32	-0.78
Error Std		3.95	7.20

Table 4.2 shows results between prediction approaches and subjective results for the case of the median. The values in parenthesis represent the difference between the prediction and subjective data at the 0.707 convergence probability point.

From this table we notice that both the mean error and standard deviation improve for the Gabor patterns when compared with table 4.1. This is due to the fact that the median does a better job with excluding outliers. Still the standard deviation is larger for Gabor patterns compared to the Symlet patterns, which clearly shows the effect that outliers have in Gabor prediction. Also, we see an improvement in standard deviation for the case of the Symlets, but this improvement is not as dramatic as the Gabor.

4.2. Banding results taking into account spatial periodicity and size

In section 4.1.1 and 4.1.2 the pooling model only combined one absolute maxima for each channel and ignored other local maximas distributed in space. Since banding patterns are periodic absolute maxima as well as local maximas or peaks exist at regular intervals that might help the human subject identify a pattern at lower contract values or it might have an effect on how offensive the pattern is to the observer after it is detected. As the envelope size of the defect patterns increases, more peaks at periodic intervals across the flat field are presented to the HVS. In our research we are trying to determine if picking multiple maximas effects the threshold estimation for the banding and graining defect patterns. One question arises. What is the optimal number of maximas we should account for in our prediction in order to better estimate the subjective results? We would expect the optimal number of maximas should be such that it minimizes the error between predictions and subjective results at the convergence probability (70.7%) point of interest.

Both the Symlet and Gabor predictions were generated for different number of maximas and the optimal number were computed for each approach. The optimal number of maximas resulting from these computations was one for Symlet and one for Gabor patterns. Thus the HVS considers only the absolute maxima when making threshold estimations. Equation 4.2.1 describes how the optimal number of maximas was computed for Symlet and Gabor approaches.

Let $P_i(0.707)$ represents the prediction at the .707 point for certain number of maximas selected. Let $S_i(0.707)$ present the subjective test result at the .707 point. The subscript *i*

represents the banding pattern of interest. The error between prediction results and subjective results for a particular number of maximas is:

$$E_k = \frac{\sum_{i=1}^{4} \left| Pi(0.707) - Si(0.707) \right|}{4} \qquad (4.2.1)$$

where k = {1,2 ,3…4) represents the number of maximas accounted for in the prediction and *i* represents the number banding defect patterns which is four for our experiment. Thus equation 4.2.1 was repeated four times first considering only one maxima, then two, three and up to a total of four maximas. The number of maximas that yielded the smallest error overall for all banding defects was considered optimal. Figure 4.9 shows the performance error difference between Symlet prediction, Gabor prediction, and subjective test for different number of maximas.

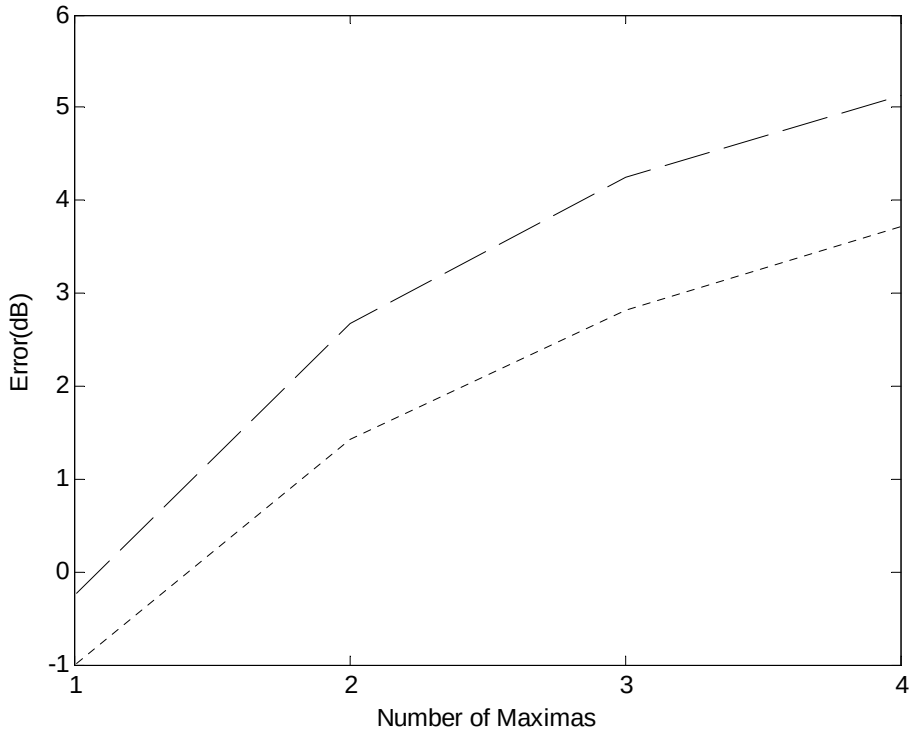

Figure 4.9 Number of maximas vs. Performance Error between Symlets prediction and Subjective results and Gabor prediction and Subjective results for the case of mean. The smallest error occurs at one maximas for Symlet and one for Gabor prediction.

From figure 4.9 we notice that the minimum number of maximas that minimize the error between prediction and subjective test is one for Symlets and one for the Gabor prediction. The graph in figure 4.9 was generated for the case of mean. Figure 4.10 shows the graph of the optimal number of maximas vs. performance error for the case of the median computation.

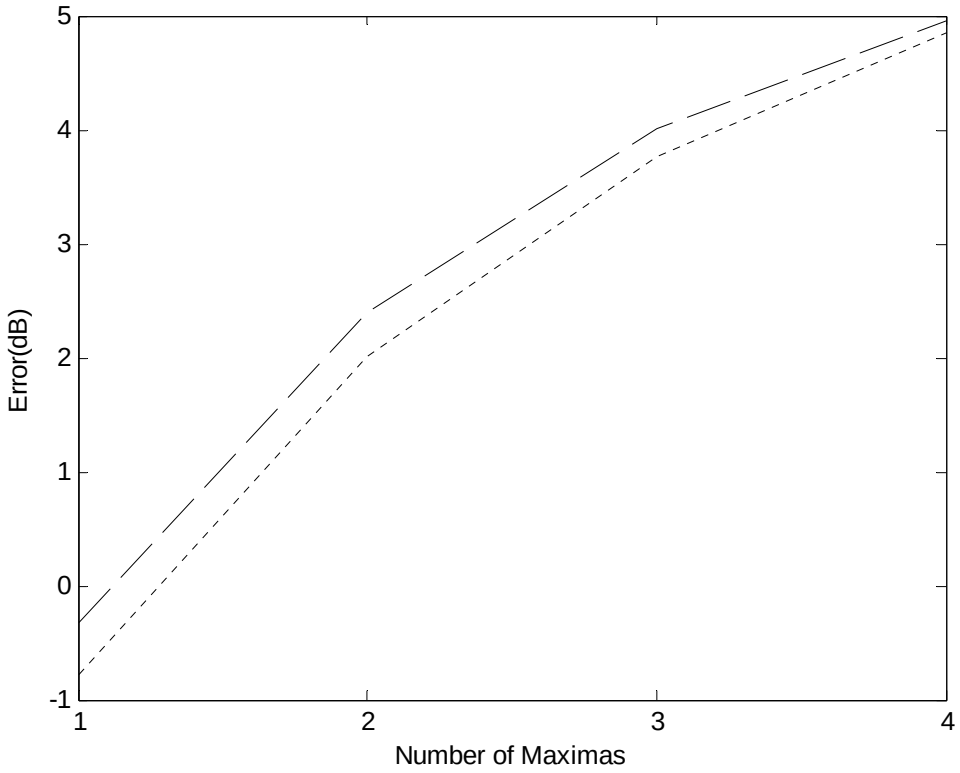

Figure 4.10 Number of maximas vs. Performance Error between Symlets prediction and Subjective results and Gabor prediction and Subjective results for the case of median. The smallest error occurs at one maximas for Symlet and one for Gabor prediction.

From Figure 4.10 we notice that the optimal number of maximas was the same for the case of the median as for the mean.

The idea of using more than one spatial point from each channel was motivated by the factor that attention and focus may play a important role in the subjective detection process. The assumption made was that the larger pattern is likely to be seen since it

occurs at multiple places in the image and possibly generates cues (especially in the case of periodic patterns) over space that aid in the detection process. From figures 4.9 and 4.10 we concluded that this assumption may not be true, thus the HVS only detects one maxima and spatial distribution does not play a significant role in threshold estimations. Still further studies should be done to determine if spatial distribution may have an impact of how offensive an already detected pattern appears to the visual system.

4.3 Experimental results for grain defect patterns

Same procedure as described in chapter 3 was used to obtain the results for graining defect patterns. The only difference between graining and banding defects is in the computation of contrast. Due to the randomness of graining defect patterns the contrast for graining patterns is computed using the root mean square as described in equation 2.2.5. The RMS was divided by the area of the defect patterns in order to obtain a true RMS, since the zeros in the image would affect the RMS results. The steps for the pooling the probability values was the same as for banding patterns. The two graining patterns results are shown below.

We noticed that the Symlet and Gabor prediction did not vary considerably compared to the subject test psychometric curve for changes in envelope size of graining patterns. Thus size does not have a dramatic affect in the subject's response to graining patterns.

4.3.1 Graining results using bootstrapping mean

As in the case of banding patterns the solid black line represents the response from subject data, the dotted line represents the prediction using Gabor decomposition approach and the dashed line represents the prediction using Symlet approach.

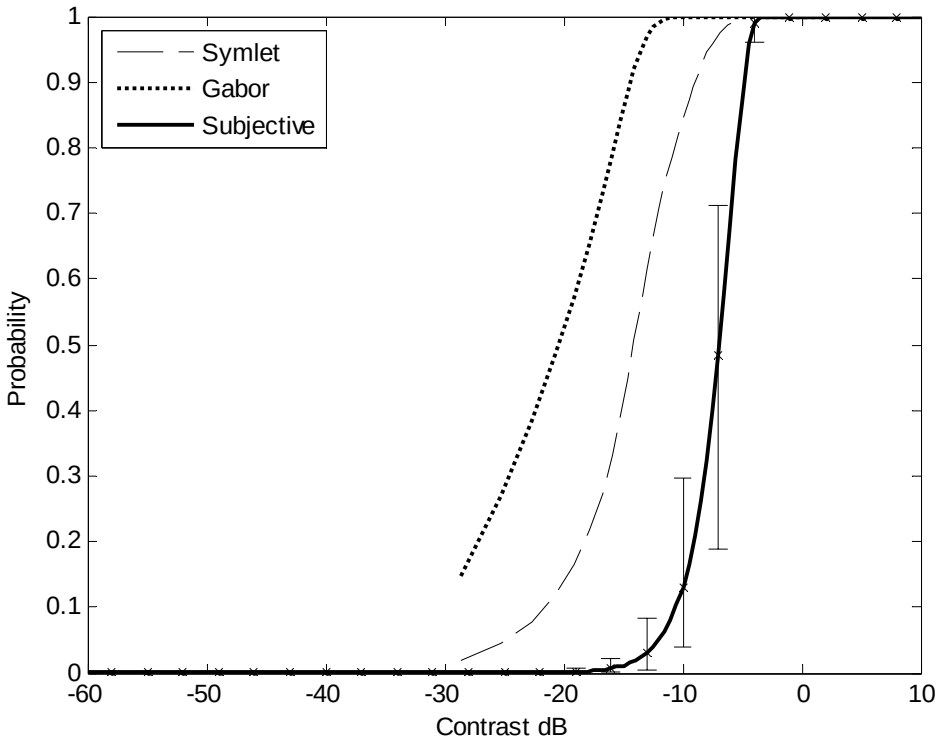

Figure 4.11 Graining 1-1 using bootstrapping mean, small envelope grain pattern

From the results of figure 4.11 we notice that the error bars are more uniform and the subject response (solid black line) is somewhat centered within the error bars. This indicates that they are not many outliers in the graining results like they were in the case of banding patterns. Both the Symlet and Gabor prediction are indicating that subjects should have observed the graining pattern at a lower contrast than they actually did. From the figure we can see that the Symlet approach (dashed line) is doing a better job predicting the response than the Gabor approach (dotted line).

The figure 4.12 shows the results for graining 1-2 pattern, the larger envelope patterns. If we compare these results with figure 4.11 we see that the predictions are somewhat similar, that indicates that size does not make such a dramatic difference in predicting graining patterns. In this figure both the Gabor and Symlet prediction are indicating that the patterns should have been observed at a lower contrast value.

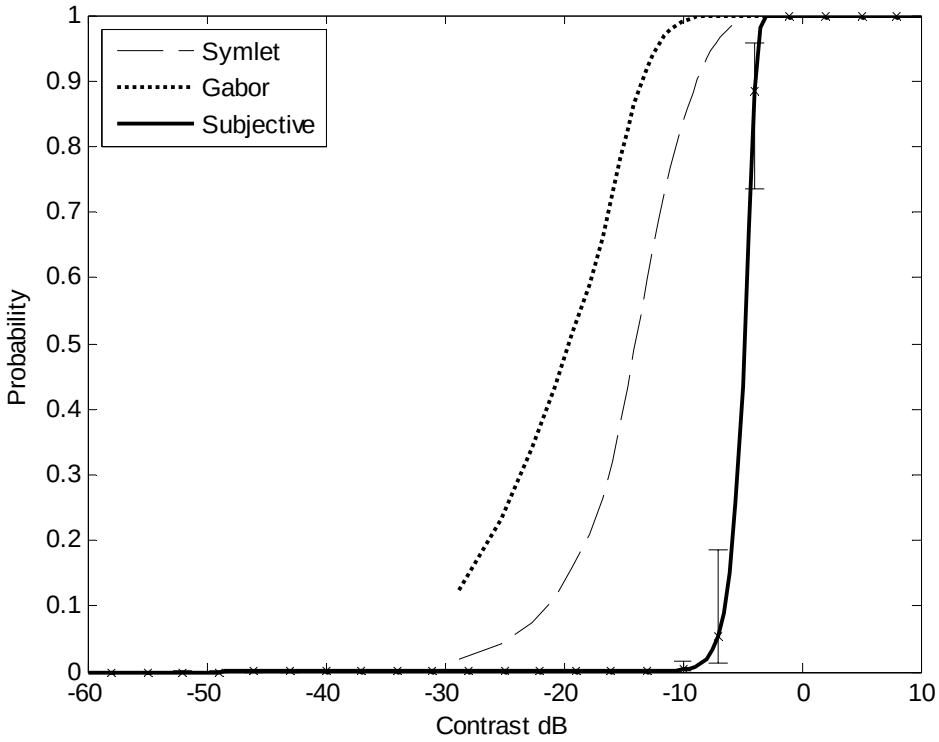

Figure 4.12 Graining 1-2 using bootstrapping mean, large envelope grain pattern

Table 4.3 shows the tabular results for graining patterns.

Table 4.3: Graining defect prediction results at the 70.7 % convergence probability. Due to non-periodicity of graining pattern only the absolute maxima is detected by the visual system. The error between subjective data and prediction is shown in parenthesis.

	Subjective(dB)	Symlet(dB)	Gabor(dB)
Graining 1-1 small envelope	-5.85	-12.03(6.17)	-17.02(11.17)
Graining 1-2 large envelope	-4.41	-11.83(7.41)	-16.21(11.80)
Mean Error(dB)		6.79	11.48

From table 4.3 we notice that the subjects had easier time to detect the smaller graining pattern than the larger one. The subjective value for the small envelope is -5.85 dB compared to -4.41 dB for the case of the large envelope. The reason why is due to the edge effect of the smaller graining pattern. The eye can better detect edges in random patterns. For larger size graining pattern the edges become smother and less detectable.

Interestingly the prediction results under the Symlet and Gabor columns in table 4.5 indicate similar results. A small spatial random patter such as graining covers more channels in frequency domain thus the probability of detection is higher than for a larger size pattern which covers fewer channels. Thus prediction supports the subjective results that HVS can detect smaller graining patterns better than larger ones. Thus this also supports our validity of prediction since the prediction is closely following the actual subject data results for the graining defect patterns.

4.3.2 Graining results using bootstrapping median

Figure 4.13 and 4.14 show the results using the bootstrapping median where only the inter-quartile values are used. Please refer to section 4.1 for more information about the median computation.

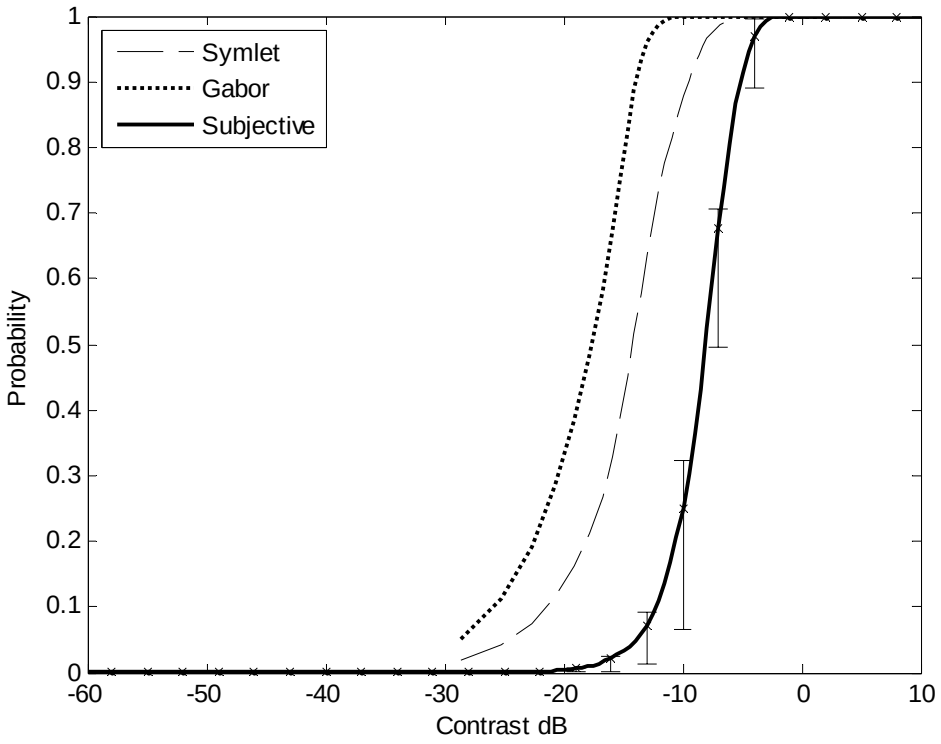

Figure 4.13 Graining 1-1 using bootstrapping median, small envelope grain pattern

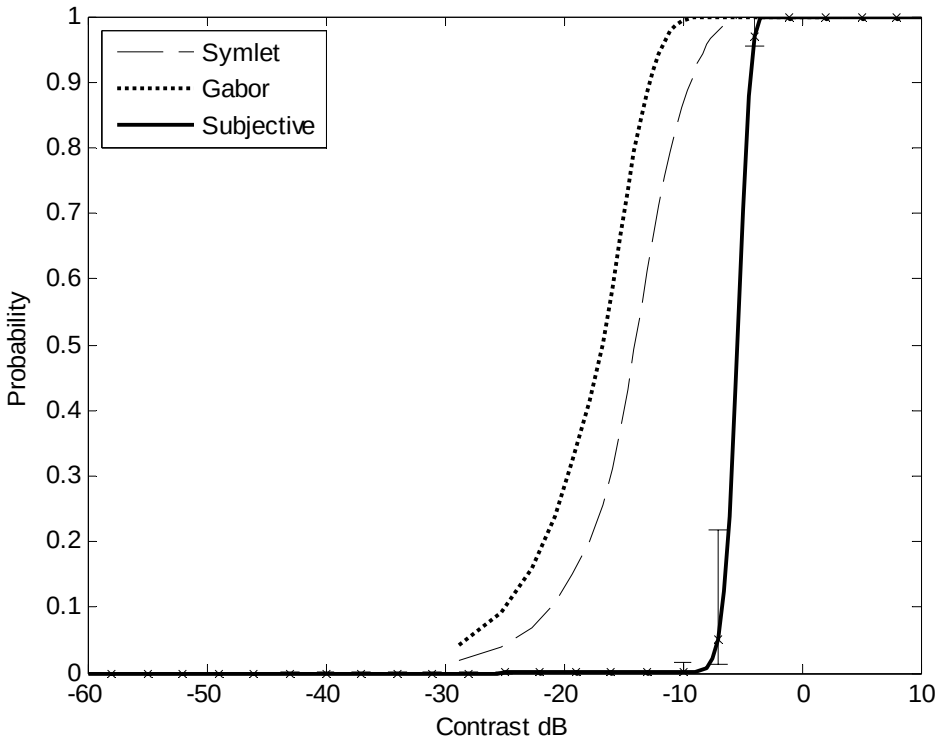

Figure 4.14 Graining 1-2 using bootstrapping median, large envelope grain pattern

For graining patterns we notice the same trend as for banding patterns. The Symlet prediction is outperforming the Gabor prediction. Table 4.6 shows these results.

Table 4. 4 Graining defect prediction results at the 70.7 % convergence probability for case of median. Due to non-periodicity of graining pattern only the absolute maxima is detected by the visual system. The error between subjective data and prediction is shown in parenthesis.

	Subjective(dB)	Symlet(dB)	Gabor(dB)
Graining 1-1 small envelope	-6.74	-12.29(5.55)	-15.63(8.89)
Graining 1-2 large envelope	-5	-12.11(7.11)	-14.91(9.91)
Mean Error(dB)		6.33	9.4

We notice a better performance when comparing the error mean of table 4.6 with table 4.5. Since there only two type of patterns considered we can not measure the standard deviation, thus only the Mean Error results are provided.

4.4 Chapter Summary

This chapter presents the results from subject testing and prediction process for print defect patterns. Each figure shows the prediction results using Gabor and Symlet approach and the subject testing results. In conclusion we notice that Symlet approach outperforms the Gabor approach in predicting the response of the HVS to print defect patterns, due to the fact that Symlets need fewer coefficients to represent defect patterns thus reducing computational errors. Thus Symlets would create a good candidate to model the HVS system. Also, we noticed that periodicity and size does not play a significant role in detection of banding defect patterns. The HVS tends to detect only the absolute peak when the envelope of the banding patterns increases. We concluded that the optimal number of maximums for the Gabor and Symlet prediction is one. We noticed the same trend for graining patterns. Size does not play a significant role for graining patterns. On the other hand we noticed that subjects can detect smaller envelope graining patterns better than larger envelope ones. This is due to the fact that HVS can detect edges better in a small graining pattern. Chapter 5 of this thesis will introduce the future work to be done in this area.

CHAPTER 5
Conclusion and Future work

This is a summary of the content of this thesis and also discusses future work that can be made to improve the prediction process of print defect patterns. Section 5.1 provides a quick summary while section 5.2 talks about future work to be done in this area.

5.1 Summary

The purpose of this thesis was to create HVS models that predict the response of the Human Visual System to print defect patterns such as banding and graining and determine which model closely approximates the detection threshold of HVS to defect patterns.

Two models were created based on Gabor and Symlet subband decompositions. A defect pattern was passed through each model and the prediction was compared to results obtained from direct subject testing. The results showed the Symlet prediction generally outperformed the Gabor prediction. That is the Symlets more accurately in predicted the human detection response to the defect patterns. The better Symlet performance was most likely due to the orthogonality property, which ensures that the pattern energy is not over counted for or undercounted in each special band. Also, a benefit of Symlets is the fact that fewer coefficients are required to represent defect patterns (pattern energy is contained in fewer coefficients) thus avoiding computational errors that occurs when pooling detection probabilities over many visual channels. Thus overall we conclude that Symlets perform better than Gabor patterns in predicting HVS response to print defect patterns. Even though it is not significant in estimating the visibility threshold (since both Gabor and Symlets where within standard deviation limits), still Symlets performed better in terms having almost half the standard deviation of the Gabor predictions over all the patterns tested. This suggests a greater robustness and performance consistency for the Symlet models.

Symlets appear to be less influenced from outliers relative to Gabor performances. This can be observed from comparing tables 4.1 thru 4.4. In table 4.1, which uses the mean in the bootstrap process (includes effects of outliers) we notice the standard deviation is lower for Symlets 4.66dB compared with 9.08dB for Gabor prediction. In table 4.2, where the median is used in the bootstrap process to limit the influence of outlier, the Symlet standard deviation reduces by less than 1 dB, while to Gabor standard deviation reduces by almost 3 dB. The same trend is observed in tables 4.2 thru 4.4. Thus Symlets provide a better representation of HVS detection of defect patterns due to their consistency in standard deviation.

This thesis extended previous work done by Venkantesh [16] by estimating the whole psychometric function and not just the threshold point of interest. Thus we obtained a general idea about the response of the visual system to the whole probability spectrum and more accurate contrast-to-probability conversions for the pooling process. A suggestion was made that spatially extended periodic patterns lowered the visibility threshold for subjective detection. After further investigation we concluded that visibility threshold is independent of spatially extended patterns.

On a similar note we noticed that size is not as significant in the case of graining patterns. For the graining patterns tested, the smaller size was actually detected better than larger size patterns. While this pattern was not expected, it also was predicted by the Symlet and Gabor prediction models. One reason for this trend is that the envelope modulation to create the smaller random increased the frequency support of defect patterns. Note that the smaller spatial support envelope has a broader frequency support. The resulting convolution in the frequency domain with the grain pattern pushed the energy into the critical visual channels improving the pattern visibility in the direct subjective tests and computationally resulting in higher detection probabilities after pooling over the visual channels.

5.2 Future Work

As outlined by ModelFest future work in this area would be to broaden the range of the defect patterns studied to include dipoles, Gaussian blobs, elongated Gabor patterns, and finally a complex image. Also future work would include creating models that detect prediction of not just banding and graining defects in gray scale but as well as complex images in color scale.

Also more insightful comparison should exist between Gabor and Symlet patterns since Gabors are wavelets, which do not form a set of orthogonal filters. So more direct studies can be done as to the advantages of orthogonality relative the response variability typically found in the human response population and pattern that are chosen to be very compact in either domain (frequency or spatial) and very distributed. This would stress orthogonality issues for double-counting contribution in overlapping visual channels.

Another improvement from this thesis would be to using a higher resolution displays since limitations existed when observing higher frequency basis functions. In this thesis we would like to test levels 2-6 of the basis functions, but due to display limitations level 2 (22.5 cpd) was unobservable by the subjects for the case of both Gabor and Symlet basis functions, even at the highest contract allowable on the monitor (saturation would begin to occur for higher contrast values).. Since this level is not present it does affect the final prediction results especially for higher frequency values. This may explain why there was a tendency to under predict human performances for the higher frequency patterns.

Another improvement to this work would be to consider the effects that spatial distribution has in qualifying a defect pattern as offensive or non-offensive. The subjective tests only examined visibility of the pattern at the threshold of detection. Supra-threshold experiments would be more important for determining/predicting the contrast levels related to the just-noticeable differences (JNDs) for different patterns. And then using the JND increments, find the artifact level on an actual image at which the user can not consistently prefer the image with no artifact to the one without (or less).

This result however may be difficult to generalize because more variables will come into play, such as the background image used and experience of the subject with printer artifacts. While this problem would be challenging in terms of modeling and experiment, it would give more practical results for understanding image quality of printer outputs.

REFERENCES

1. Carney, T., Klein, S. A., Tyler, C. W., Silverstein, A. D., Beutter, B., Levi, D., Watson, A. B., Reeves, A. J., Norcia, A. M., Chen, C.-C., Makous, W. & Eckstein, M. P. , " The Development of an image/threshold database for designing and testing human vision models", *SPIE*, 1999, pg. 248-257

2. S. Western, KL Lagendijk, and J. Biemond. "Perceptual Image Quality based on a Multiple Channel HVS Model". *ICASSP*, 1995, pp. 2351-2354.

3. S. Daly, "The visible differences predictor: An algorithm for the assessment of image fidelity", Digital Images and Human Vision, A. B. Watson (Ed.), Chapter 14, *MIT Press*, 1993, pg. 179-205

4. D. J. Heeger and P. C. Teo, "A model of perceptual image fidelity", *Proceedings of IEEE International Conference on Image Processing*, Oct. 23 – 26 1995, Washington, D.C., USA, pg. 343-345.

5. J Lubin, "A visual discrimination model for imaging systems design and evaluation", Vision models for Target Detection and Recognition, E. Peli (Ed.), Singapore: *World Scientific*, 1995, pg. 245 – 283.

6. K.D.Donohue, C. Cui, and M.Vijay Venkatesh, "Wavelet Analysis of Print Defects", *IS&T*, Portland, OR, 2002, pg. 42-47.

7. A. B. Watson, "DCT quantization matrices visually optimized for individual images", Human Vision, Visual Processing, and Digital Display IX, Proc. *SPIE*, 3644, 1999, 168-174.

8. B. A. Wandell, Foundations of Vision, Sinauer Associates, Inc., 1995.

9. Daugman, J. "Two-dimensional spectral analysis of cortical receptive field profiles", *Vision Research*, Vol. 20, 1980, pg. 847-856.

10. Daugman, J. "Six formal properties of two-dimensional anisotropic visual filters: structural principles and frequency/orientation selectivity," *IEEE Trans*. Systems, Man, Cybernetics SMC, Vol. 13, No 5, 1983, pg. 882-906.

11. Marcelja, S. "Mathematical description of the responses of simple cortical cells", *Journal of Optical Society of America*, Vol. 70, No 11, 1980, pg. 1297-1300

12. Paul J. Kane, Theodore F. Bouk, Peter D. Burns, and Andrew D. Thompson, "Quantification of Banding, Streaking and Grain in Flat Field Images", *IS&T*, Portland, OR, 2000, pg. 79-83.

13. John C. Briggs, Mike Murphy, and Yichuan Pan, “Banding Characterization for Inkjet Printing”, *IS&T*, Portland, OR, 2000, pg. 84-88.

14. Jones, J.P., and Palmer, L.A. "An evaluation of the two-dimensional Gabor filter model of simple receptive fields in cat striate cortex", *Journal of Neurophysiology,* Vol. 58, No 6, 1987, pg. 1233-1258.

15. Stork, D.G., and Wilson, H.R. "Do Gabor functions provide appropriate descriptions of visual cortical receptive fields?" *Journal of Optical Society of America*, Vol. 8, 1990, pg. 1362-1373.

16. Venkatesh, Vijay, “Wavelet and Sined based analysis of print quality evaluations”, Master Thesis, University of Kentucky, February 2004.

17. Weber E H, De Pulsu, Resorptione, Auditu et Tactu (Leipzig: Koehler), 1834.

18. G.E.Legge and J.M.Foley, “Contrast masking in human vision”, *JOSA*, Vol.70, No. 12, December, 1980, pg. 1458-1471.

19. Chengwu Cui, Dingcai Cao, and Shaun Love, “Measuring Visual Threshold of Inkjet Banding”, *IS&T*, Montreal, Canada, 2001, pg. 84-89.

VITA

Elios Klemo was born on October 02 1979 in Tirane, Albania. He received his bachelor's degree in Electrical Engineering from the University of Kentucky, USA in 2002 with Magna Cum Laude honors. He currently works for Lexmark International in the Research and Development branch. He is a member of Golden Key International Honor Society and HKN Honor Society. His research interests are in Image and Signal Processing and development of algorithms that mimic human vision.